MASTER'S DEGREE THESIS

MSc in Mathematics Engineering

Title: Precessing models and eventual links with galaxy warps

Author: Daniel Barajas

Advisor: Josep J. Masdemont

Department: Matemàtica Aplicada 1

Academic year: 2010-2011

Facultat de Matemàtiques i Estadística

UNIVERSITAT POLITÈCNICA DE CATALUNYA

Universitat Politècnica de Catalunya
Facultat de Matemàtiques i Estadística

Master's Degree Thesis

PRECESSING MODELS AND EVENTUAL LINKS WITH GALAXY WARPS

Daniel Barajas

Advisor: Josep J. Masdemont

Abstract

Keywords: The Restricted Three Body Problem, precession, critical points, periodic orbits, invariant manifolds, rigid body dynamics, galactic models, galaxy warps.

The Restricted Three Body problem is a basic model in celestial mechanics and it has been extensively used in the design of some spatial missions. Sometimes, the designers of these missions consider other similar models which are perturbations of this because the physical reality is more complex and they have to take into account the influence of other physical phenomena. In this work, the idea of the Restricted Three Body problem is adapted to a precession phenomenon. This precession is considered in different ways and, as a result, different models are obtained. It will be important to analyze the models by computing the invariant objects like critical points, periodic orbits and invariant manifolds. Another objective of this work is to see how a precessing models can be useful when applied to galactic dynamics, which is an important field where the results of celestial mechanics have been widely used. In this case, a precessing model can be a first approximation to explain the warps observed in some galaxies.

0. Contents

1. Introduction

1.1 Objectives of the present work

One of the purposes of dynamical systems theory is to study the long-term behaviour of an evolving system. It is usually a mathematical way of describing a physical reality. There are two types of dynamical systems depending on whether the time is discrete or continuous. More precisely, a continuous-time dynamical system consists of a space X and a family of maps $f^t : X \longrightarrow X$, $t \in \mathbb{R}$, that forms a one-parameter group, i.e., $f^{t+s} = f^t \circ f^s$ and $f^0 = Id$. Here, we will assume that $X = \mathbb{R}^3$ and the family of maps are obtained from ordinary differential equations (ODE) that can be reduced to a first order ODE system. These type of equations have been thoroughly studied and we have lots of results at our disposal. Moreover, there are well known numerical procedures which allow us to compute the solutions of these equations. Critical points, periodic orbits, tori, invariant manifolds, all of them are invariant objects under the flow (the solution of the ODE), which means that any state being in the object will remain in it in the future. In celestial mechanics, these objects are very important for this reason. In recent years, some spacecrafts have been placed in periodic orbits near the critical points.

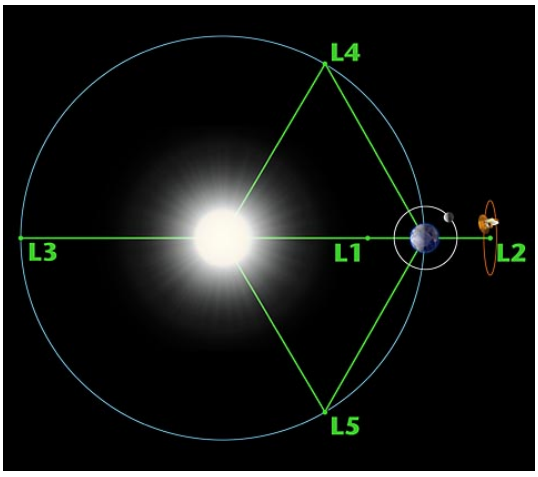

Figure 1.1. Spacecraft in a periodic orbit near Earth-Sun L_2 point.

For example, the SOHO project (Solar and Heliospheric Observatory) from ESA and NASA considers a spacecraft which describes a halo orbit around the critical point L_1 of the Earth-Sun Restricted Three Body Problem. This critical point is located over the line which connects the Earth and the Sun (figure 1.1). For this reason, a periodic orbit near this point becomes an excellent observatory of the solar activity. Some of the advantages that suppose having the spacecraft in this trajectory are the following:

- A permanent observation of the Sun. The emplacement is optimum for a direct observation of the Sun's activity.
- A saving of energy. Since the halo orbit is a natural motion due to the gravity of the Sun and the Earth, this permits a reduction of the waste of energy. Moreover, the invariant stable and unstable manifolds are used as "spatial highways" in order to travel from/to the Earth.
- Solar interferences are avoided. Since the radius of the orbit is big enough, radiation is not a problem for the communications with the Earth.

Apart from the periodic orbits and the critical points, the invariant manifolds are also important in the dynamics. For example, in some cases, these manifolds are paths in the space permitting a natural motion from a particular point to another. As we will see later, this implies important consequences in the reality represented by the model.

In the present work, we are going to construct some models with the objective of studying how a precession movement affects the critical points, the periodic orbits and the invariant manifolds of some dynamical systems that are usually referred to as planars. The term planar is not used in the sense of being defined in a plane but of having a clear planar component, although the system is defined in the space. Roughly speaking, the precession is defined as a change in the orientation of the rotation axis of a body. An example of this is found in the Earth's motion. The Earth is submitted to a precession phenomenon which makes the axis of rotation to describe a cone. A consequence of the precession is a changing pole star. Polaris, in the constellation Ursa Minor, is the star that nowadays marks quite well the position of the north celestial pole. However, this motion is substituting the pole star in a cycle of about 26000 years. This motion, applied to some models, acts as a perturbation and the invariant objects are altered. The models considered in this work will be simple and each one built in a specific way in order to modelize this phenomenon. In this way, there will be some sections in which the critical points, the periodic orbits and the invariant manifolds related to these orbits will be computed using numerical procedures. The Restricted Three Body Problem will be the model to bear in mind as all the considered models will have many similarities. Therefore it is important to know some previous things about it before starting the construction of the precessing models. Next section summarises the basic from this model. Then, we present a section with the objective of getting an insight into the galaxy shape classification and galactic dynamics since, once we will have modeled the precession phenomenon, an important purpose of this work will be to try to explain some of the observed physical phenomena in the galactic context. Concretely, we are interested in some galaxies showing a curious behaviour.

Most of the observed galaxies, like which is shown in figure 1.2, are seen from the Earth in a position that allows us to distinguish its structures like spiral arms or rings.

Figure 1.2. Galaxy M81 photographed by Hubble telescope.

Figure 1.3. Galaxy NGC 5866 photographed by Hubble telescope.

However, other galaxies are presented in an edge-on position, like in figure 1.3, which permit us to see the flatness of its disk. On August 2, 2001 the Hubble site published a photograph capturing a spiral edge-on galaxy (figure 1.4). Galaxy ESO 510-G13 reveals an unusual behaviour: its disk is warped. The reason of this twist is not known yet. Some theories suggest that it is caused by gravitational forces produced by a collision with a nearby galaxy. A sign that supports this theory is the presence of bright clouds of blue stars in the outer regions of ESO 510-G13. These stars indicate that new stars are being formed and astronomers believe that this is caused by the interaction of two galaxies.

Figure 1.4. Galaxy ESO 510-G13 photographed by Hubble telescope.

Some studies reveal that the Milky Way could also have a warp in its disk but lower in magnitude. The origin, again, is not clear. It may be caused by the Magellanic Clouds, satellite galaxies of ours, and an halo of dark matter, an extragalactic magnetic field or the accretion of intergalactic medium over the galactic disk. In [13] the authors eliminate both, the first and the second option, and supports the third.

The rest of the work is structured as follows. In chapter 2 we present a first model developed from the Restricted Three Body Problem. We expose the analytical procedure to obtain the non-autonomous system of equations of motion. Chapter 3 is intended to explain some basic results in rigid body dynamics addressing the concept of precession. Then, we find our second model, non-autonomous too, based on two spheres which considers an applied torque. After that, a similar model but without having torque is presented. This model can be thought as autonomous under some assumptions. Last part of chapter 3 adapts this model without torque to the galactic context. In chapter 4 we develop some methods in order to analyse the four models presented. There, we compute critical points, periodic orbits, curves and surfaces of null velocity and, finally, stable and unstable invariant manifolds. Chapter 5 concludes this work.

1.2 The Restricted Three Body Problem

In the Restricted Three Body Problem model (from now on, RTBP) two massive bodies, called primaries, move in a circle or an ellipse around the origin and a third one, with negligible mass, moves affected by the gravity of them.

The equations of this model describe the motion of this third body and are obtained by means of the use of a non-inertial reference frame (synodic frame). This frame is revolving with respect to an inertial reference frame (sidereal frame) in order to fix the coordinates of the primaries (figure 1.5).

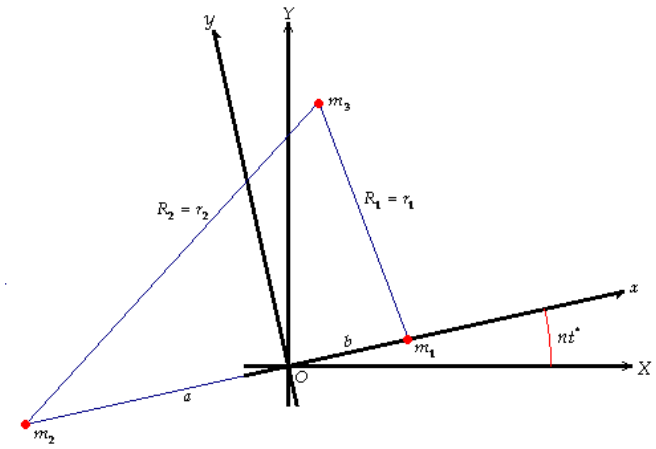

Figure 1.5. Relation between the two frames involved in the RTBP. x and y axes are turning on the origin whereas X and Y are fixed.

After few assumptions and using the Newton's Law of Universal Gravitation the equations are reduced to

$$\begin{aligned} \ddot{x} - 2\dot{y} - x &= U_x, \\ \ddot{y} + 2\dot{x} - y &= U_y, \\ \ddot{z} &= U_z, \end{aligned}$$

where

$$U(x, y, z) = \frac{1-\mu}{r_1} + \frac{\mu}{r_2}$$

is the potential and

$$\begin{aligned} r_1 &= \sqrt{(x-\mu)^2 + y^2 + z^2}, \\ r_2 &= \sqrt{(x-\mu+1)^2 + y^2 + z^2}, \end{aligned}$$

the distances of the third body with respect to the primaries. Many times the system is written using the effective potential $\Omega(x, y, z)$:

$$\begin{aligned} \ddot{x} - 2\dot{y} &= \Omega_x, \\ \ddot{y} + 2\dot{x} &= \Omega_y, \\ \ddot{z} &= \Omega_z, \end{aligned}$$

$$\Omega(x, y, z) = \frac{1}{2}\left(x^2 + y^2\right) + \frac{1-\mu}{r_1} + \frac{\mu}{r_2} + \frac{1}{2}\mu(1-\mu).$$

Finally, the corresponding first order ODE system is

$$\begin{aligned} \dot{x}_1 &= x_4, \\ \dot{x}_2 &= x_5, \\ \dot{x}_3 &= x_6, \\ \dot{x}_4 &= 2x_5 + \Omega_{x_1}, \\ \dot{x}_5 &= -2x_4 + \Omega_{x_2}, \\ \dot{x}_6 &= \Omega_{x_3}, \end{aligned}$$

being $x_1 = x$, $x_2 = y$ and $x_3 = z$.

The only parameter in this model, μ, is related to the masses of the primaries. μ represents the mass of the less massive primary whereas the mass of the most massive primary is $1 - \mu$. Therefore, the total mass of the problem is normalized to 1. Moreover, the values of μ are restricted to $[0, \frac{1}{2}]$. The degenerate case $\mu = 0$ can be thought as a two body problem whereas $\mu = \frac{1}{2}$ is a symmetric distribution of the total mass, being the primaries equal. The location of the bodies is expressed by means of this parameter (figure 1.6).

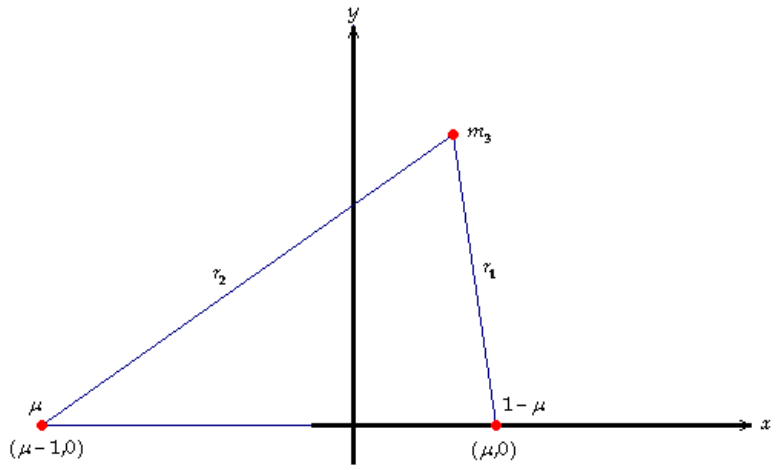

Figure 1.6. Coordinates of the primaries in the synodic frame of reference.

The equations of motion have five critical points, L_1, L_2, L_3, L_4 and L_5, divided into two types: the collinear points and the triangular points. The three collinear points are located in the axis where the primaries are located whereas the two triangular points form equilateral triangles with vertices the two primaries and the critical point (figure 1.7).

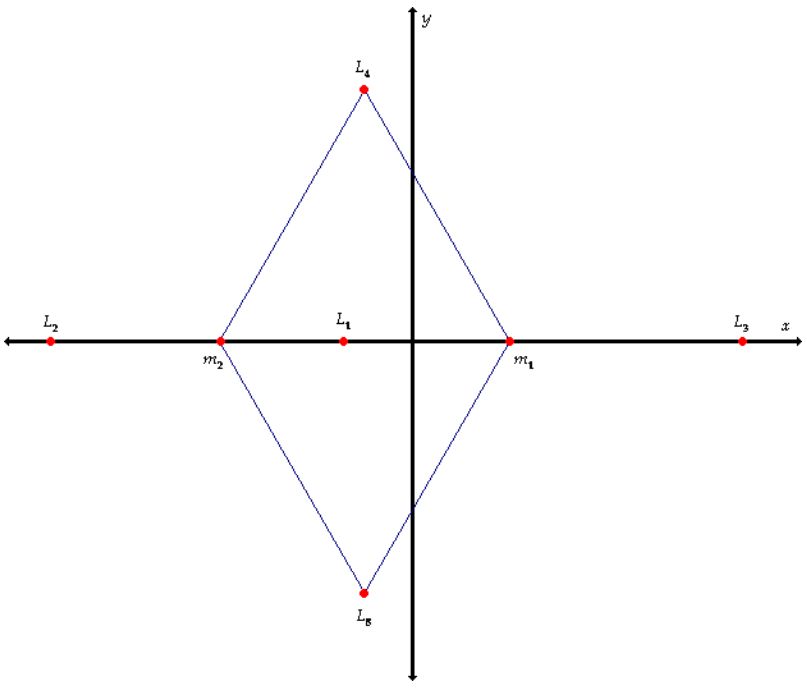

Figure 1.7. Disposition of the primaries and the critical points.

There are a lot of results concerning this model about the stability of the critical points, the periodic orbits that exists near them and their stability, tori, manifolds, etc. The reader could find lots of further information just by doing a research on internet or looking up the wide variety of papers dealing with this model. A main reference on this matter is [21].

In this work, we are going to modify the RTBP (introducing some forces or just

changing the classic conception) in order to study its characteristics. Some calculations will be made to study how the model changes with the introduction of the precession phenomenon. For example, in some models the critical points found in the RTBP are replaced by periodic orbits, the periodic orbits by tori and so on. It will be also important to see how the stable and unstable manifolds of periodic orbits behave under this new situation.

Remark. In all the models considered in this work where the parameter μ is present, it will take the value corresponding to a symmetric distribution of the masses, i.e., $\mu = \frac{1}{2}$.

1.3 Galaxy shape classification

A galaxy is any of a vast number of star systems held together by gravitational attraction. Its shape can be asymmetric (an irregular galaxy) or, more usually, symmetric (a regular galaxy). The Hubble sequence is a classification invented by Edwin Hubble in 1926 which divides regular galaxies into elliptical, lenticular and spiral galaxies based on their visual appearance.

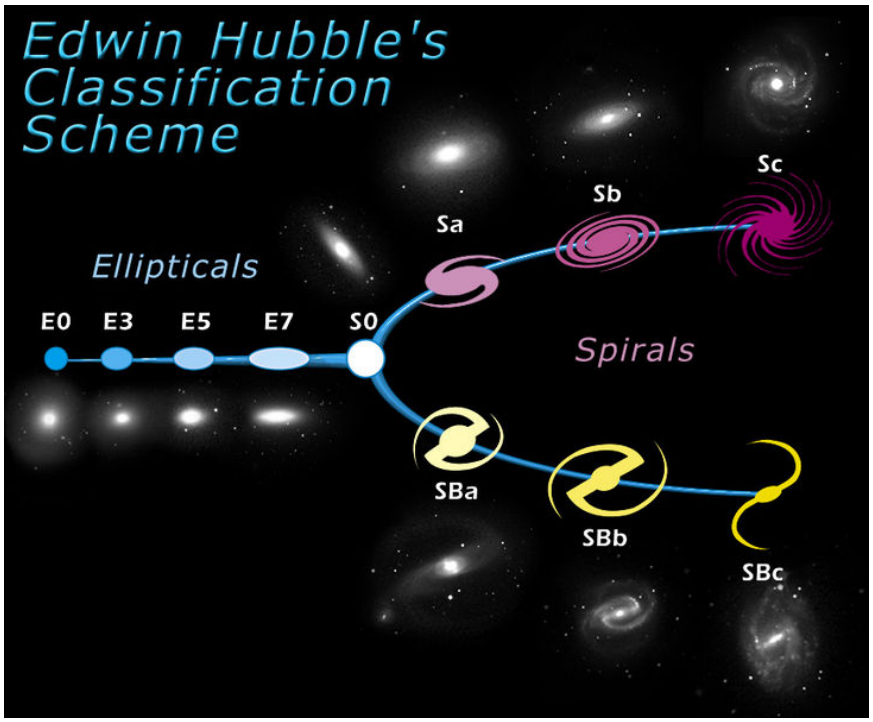

Figure 1.8. Hubble sequence.

On the left side lie the elliptical galaxies. In photographic images they seem ellipses and are designated with the letter E followed by a number which denotes its degree of ellipticity. This number is ten times the ellipticity calculated as $e = 1 - \frac{b}{a}$, being a and b the length of the semi-major and semi-minor axis respectively. Elliptical galaxies are presented as galaxies with a low rate of stars formation activity, formed by old low-mass stars and a dispersed interstellar medium. They are believed to be a $10 - 15\%$ of the

galaxies in our Local Universe.

On the right side of figure 1.8 there are two branches which comprise spiral galaxies. These galaxies are characterized by having a disk (planar in most of the cases), a concentration of stars which form some spiral arms (usually two) and a bulge in the centre. In the upper branch lies the regular spiral galaxies whereas the lower contains those spiral galaxies showing a bar-like structure in the middle. These so-called barred galaxies are roughly the 50% of the observed spiral galaxies. Spiral galaxies are designed with the letter S if they belong to the upper branch or SB if they belong to the lower one followed by the letter a, b, or c depending on their spiral structure. Spiral arms are the place where new hot stars are formed and, because of this, this structures are brighter and clearly distinguishable from the disk.

At the centre of the classification where the two branches meet lies the lenticular galaxy type. This class consists of a disk-like structure with a bulge in the centre like spiral galaxies, however, lenticulars do not have an evident spiral arm structure.

An extension of Hubble classification was done by Gérard de Vaucouleurs in 1959. He argued that Hubble sequence did not represent the whole variety of observed galaxies because it was based only on the density of the spiral arms and the presence of a bar. In addition to this, Vaucouleurs classification divides the galaxies into two classes depending on the presence or absence of ring-like structures. Since Vaucouleurs', subtle extensions have been made. For example, ring-like structures in barred galaxies are divided into three groups: nuclear rings, inner rings and outer rings. Nuclear rings are located near the nucleus, inner rings surround the bar and outer rings are the largest and the most spectacular. The notation used for a galaxy which has inner rings is r whereas for outer rings is whether R_1, if the major axis of the ring is perpendicular to the bar, or R_2, if the major axis is the same as the bar one. There are another case, denoted as R_1R_2, when the ring has two components, one perpendicular and other parallel. For further information see [5], [6], [7], [8] and [9].

In recent years, many efforts have been made to explain the significant structures observed in some galaxies. These studies were mainly focused in barred galaxies. In the case of ring-like structures, Schwarz ([18], [19], [20]) proved that this type of structures arise near Lindblad resonances (a kind of resonance which affects the stars at a certain distance from the centre of the galaxy and depending on the radial component of its orbital velocity). In the case of spiral arms, Danby showed that the gravitational potential corresponding to the bar is one of the principal causes in its formation. He also said that some orbits departing from the ends of the bar have the same shape of the spiral arms and, in other cases, these can form ring-like structures too. Most of the researchers coincide that spiral arms and rings are produced by the gravitational field of the galaxy.

There are recent papers which connect the formation of both, spiral arms and rings. In [16] the authors propose a new theory to explain the formation of rR_1 ring structures. It is suggested that these rings are formed by material from the stable and unstable invariant manifold associated with the Lyapunov orbits around the equilibrium points of a barred galaxy. In [17] the same basic idea is developed for other models

based on simple barred galaxy potentials. In that paper, for each model they vary one parameter of the potential and fix the others. Then, the structure corresponding to this potential is computed and the influence of each parameter in the final shape can be observed. Among other results, they found that the presence (or absence) of homoclinic or heteroclinic orbits is determinant in the formation of R_1, R_2 or R_1R_2 rings. In [1] the same group of researchers answer some important questions related to their previous work. One of these questions is to determine a priori the morphology of a galaxy from its potential, in case of being possible. In [2] there are some qualitative comparisons between the theoretical results and the observations to check the validity of the work. Finally, in [3] further comparisons are made and the authors show that the theory used in these five papers can explain other galaxy features like the ansae, which is a concentration of material near the ends of the bar, or the bar shape.

As it is shown in the papers referred above, a well developed model can successfully explain the forms we observe in the different galaxies. One advantage of that model is the simplicity of its background, since the applied tools are well known in celestial mechanics. In this context there are many results which can be translated to the context of galactic dynamics.

2. Forcing the RTBP

We start with a model which is artificial but quite simple. We say it is artificial because it is more academic than realistic[1] but it will be useful to begin with our study due to its simplicity. It consists in considering the RTBP but including a precession phenomenon which we assume that is caused by an external influence. The precession will be caused by assuming that the plane where the primaries move has an inclination i and is suffering a rotation of angular velocity ω (figure 2.1). This type of motion may remind us a gyroscope so this model could be termed as a Gyroscopically Precessing RTBP (GP-RTBP). The main disadvantage of it will be the difficulty in finding the relation between the external cause and the force which cause the precession.

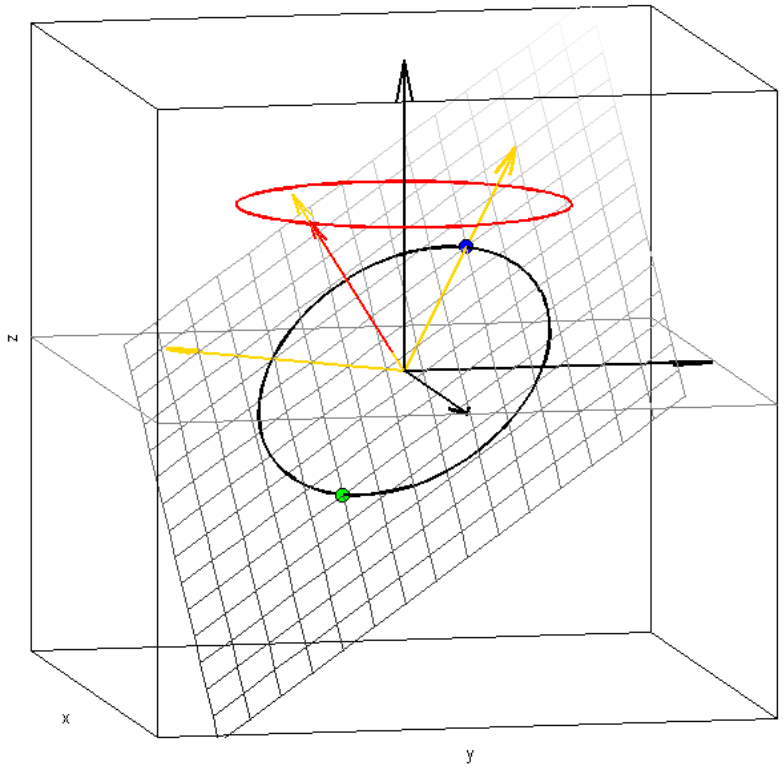

Figure 2.1. Snapshot of the motion of synodic coordinates with respect to the sidereal ones. Sidereal coordinates (black), synodic coordinates (yellow) and angular momentum (red).

The procedure explained in next sections in which we find the equations of the motion of a

[1] In the sense that two particles cannot move in this way only under the effect of the Law of Gravitation.

body submitted to the gravity of other two will be a standard procedure in the models we present afterwards. Hence the importance of having a quite simple model to understand all the steps.

2.1 Transformation of coordinates

We are looking for a similar formulation to the RTBP in which two reference systems are used: the sidereal (inertial) and the synodic (non-inertial). Like in the RTBP we define, first of all, the sidereal and the synodic frames of reference. The first one is fixed while the second one fixes the coordinates of the primaries. Both frames have the centre of mass in the origin. The sidereal axes are $\hat{X}$, $\hat{Y}$ and $\hat{Z}$, and $\hat{x}$, $\hat{y}$ and $\hat{z}$ for the synodic axes. It is necessary to define the transformation of coordinates between these frames. Let XYZ and xyz be two frames where xyz is obtained doing some rotations to XYZ frame. For instance, consider the following particular case represented in figure 2.2.

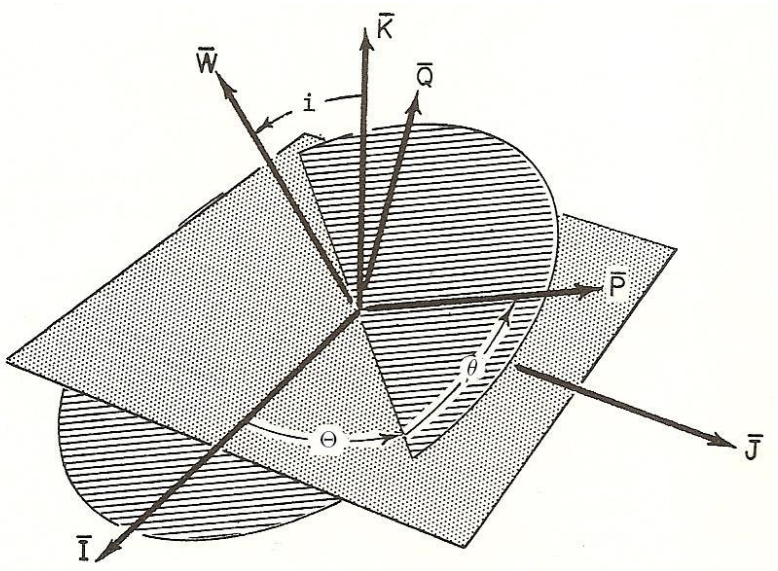

Figure 2.2. Sidereal and synodic frames and Euler angles. From [4].

We can think the transformation of coordinates as a composition of three rotations:

1. A rotation that turns around Z axis an angle Θ.
2. A rotation that turns around X axis an angle i.
3. A rotation that turns around Z axis an angle θ.

The rotation of angle Θ around Z axis (which has unit vector $\bar{K}$) can be represented by means of the matrix $R_{Z(\Theta)}$:

$$\mathbf{R}_{Z(\Theta)} = \begin{pmatrix} \cos\Theta & \sin\Theta & 0 \\ -\sin\Theta & \cos\Theta & 0 \\ 0 & 0 & 1 \end{pmatrix}.$$

In the same way

$$\mathbf{R}_{X(i)} = \begin{pmatrix} 1 & 0 & 0 \\ 0 & \cos i & \sin i \\ 0 & -\sin i & \cos i \end{pmatrix},$$
$$\mathbf{R}_{Z(\theta)} = \begin{pmatrix} \cos\theta & \sin\theta & 0 \\ -\sin\theta & \cos\theta & 0 \\ 0 & 0 & 1 \end{pmatrix}.$$

Therefore, the transformation of coordinates is

$$\mathbf{v}_{\bar{I}\bar{J}\bar{K}} = \mathbf{R}^{-1}_{Z(\Theta)}\mathbf{R}^{-1}_{X(i)}\mathbf{R}^{-1}_{Z(\theta)}\mathbf{v}_{\bar{P}\bar{Q}\bar{W}},$$

that is,

$$\mathbf{v}_{\bar{I}\bar{J}\bar{K}} = \begin{pmatrix} \cos\Theta\cos\theta - \sin\Theta\sin\theta\cos i & -\cos\Theta\sin\theta - \sin\Theta\cos\theta\cos i & \sin\Theta\sin i \\ \sin\Theta\cos\theta + \cos\Theta\sin\theta\cos i & -\sin\Theta\sin\theta + \cos\Theta\cos\theta\cos i & -\cos\Theta\sin i \\ \sin\theta\sin i & \cos\theta\sin i & \cos i \end{pmatrix} \mathbf{v}_{\bar{P}\bar{Q}\bar{W}},$$

where $\mathbf{v}_{\bar{I}\bar{J}\bar{K}}$ and $\mathbf{v}_{\bar{P}\bar{Q}\bar{W}}$ are points or vectors whose coordinates are in XYZ and xyz respectively.

2.2 GP-RTBP equations of motion

The situation in our model is similar to figure 2.2 but introducing some changes. Since the synodic frame fixes the coordinates of the primaries, the angle θ of figure 2.2 must be nt^*, where n is the mean motion of the primaries. Θ must also depend on time due to the rotation of angular velocity ω, i.e., $\Theta = \omega t^*$.

The objective now is to find the equations of motion of a third body in a model in which the primaries have fixed coordinates, like in the RTBP. Let us consider $(\hat{X}, \hat{Y}, \hat{Z})^T$ as the coordinates of third body in sidereal reference and $(\hat{x}, \hat{y}, \hat{z})^T$ as the coordinates in synodic reference. Both are related by the transformation

$$\begin{pmatrix} \hat{X} \\ \hat{Y} \\ \hat{Z} \end{pmatrix} = \mathbf{R^{-1}} \begin{pmatrix} \hat{x} \\ \hat{y} \\ \hat{z} \end{pmatrix},$$

where

$$
\begin{aligned}
\mathbf{R^{-1}} &= \begin{pmatrix} \mathbf{R^{-1}_{1,1}} & \mathbf{R^{-1}_{1,2}} & \mathbf{R^{-1}_{1,3}}, \\ \mathbf{R^{-1}_{2,1}} & \mathbf{R^{-1}_{2,2}} & \mathbf{R^{-1}_{2,3}} \\ \mathbf{R^{-1}_{3,1}} & \mathbf{R^{-1}_{3,2}} & \mathbf{R^{-1}_{3,3}} \end{pmatrix}, \\
\mathbf{R^{-1}_{1,1}} &= \cos\omega t^* \cos nt^* - \sin\omega t^* \sin nt^* \cos i, \\
\mathbf{R^{-1}_{1,2}} &= -\cos\omega t^* \sin nt^* - \sin\omega t^* \cos nt^* \cos i, \\
\mathbf{R^{-1}_{1,3}} &= \sin\omega t^* \sin i, \\
\mathbf{R^{-1}_{2,1}} &= \sin\omega t^* \cos nt^* + \cos\omega t^* \sin nt^* \cos i, \\
\mathbf{R^{-1}_{2,2}} &= -\sin\omega t^* \sin nt^* + \cos\omega t^* \cos nt^* \cos i, \\
\mathbf{R^{-1}_{2,3}} &= -\cos\omega t^* \sin i, \\
\mathbf{R^{-1}_{3,1}} &= \sin nt^* \sin i, \\
\mathbf{R^{-1}_{3,2}} &= \cos nt^* \sin i, \\
\mathbf{R^{-1}_{3,3}} &= \cos i.
\end{aligned}
$$

The equations of motion in $\hat{X}\hat{Y}\hat{Z}$ frame are:

$$
\begin{cases}
\dfrac{d^2\hat{X}}{dt^{*2}} = \dfrac{\partial\hat{\mathcal{U}}}{\partial\hat{X}} \\
\dfrac{d^2\hat{Y}}{dt^{*2}} = \dfrac{\partial\hat{\mathcal{U}}}{\partial\hat{Y}} \\
\dfrac{d^2\hat{Z}}{dt^{*2}} = \dfrac{\partial\hat{\mathcal{U}}}{\partial\hat{Z}}
\end{cases}, \tag{2.1}
$$

where

$\hat{\mathcal{U}} = k^2\left(\dfrac{m_1}{\hat{R}_1} + \dfrac{m_2}{\hat{R}_2}\right)$ is the gravitational potential and k^2 the gravitational constant,

$\hat{R}_1 = \sqrt{(\hat{X}-\hat{X}_{P1})^2 + (\hat{Y}-\hat{Y}_{P1})^2 + (\hat{Z}-\hat{Z}_{P1})^2}$ and

$\hat{R}_2 = \sqrt{(\hat{X}-\hat{X}_{P2})^2 + (\hat{Y}-\hat{Y}_{P2})^2 + (\hat{Z}-\hat{Z}_{P2})^2}$.

Therefore

$$
\begin{aligned}
\frac{\partial\hat{\mathcal{U}}}{\partial\hat{X}} &= -k^2\left[m_1\frac{(\hat{X}-\hat{X}_{P1})}{\hat{R}_1^3} + m_2\frac{(\hat{X}-\hat{X}_{P2})}{\hat{R}_2^3}\right], \\
\frac{\partial\hat{\mathcal{U}}}{\partial\hat{Y}} &= -k^2\left[m_1\frac{(\hat{Y}-\hat{Y}_{P1})}{\hat{R}_1^3} + m_2\frac{(\hat{Y}-\hat{Y}_{P2})}{\hat{R}_2^3}\right], \\
\frac{\partial\hat{\mathcal{U}}}{\partial\hat{Z}} &= -k^2\left[m_1\frac{(\hat{Z}-\hat{Z}_{P1})}{\hat{R}_1^3} + m_2\frac{(\hat{Z}-\hat{Z}_{P2})}{\hat{R}_2^3}\right].
\end{aligned}
$$

The coordinates of the primaries $\hat{\mathbf{u}}_{\mathbf{P1,P2}} = (\hat{X}_{P1,P2}, \hat{Y}_{P1,P2}, \hat{Z}_{P1,P2})^T$ can be obtained using the transformation with the synodic coordinates: $\hat{\mathbf{v}}_{\mathbf{P1}} = (\hat{x}_{P1}, \hat{y}_{P1}, \hat{z}_{P1})^T = (b, 0, 0)^T$ and

$\hat{\mathbf{v}}_{\mathbf{P2}} = (\hat{x}_{P2}, \hat{y}_{P2}, \hat{z}_{P2})^T = (-a, 0, 0)^T$. We define $\hat{\mathbf{u}} = (\hat{X}, \hat{Y}, \hat{Z})^T$ and $\hat{\mathbf{v}} = (\hat{x}, \hat{y}, \hat{z})^T$. The left hand side of equations (2.1) can be thought as $\ddot{\hat{\mathbf{u}}}$. Using the transformation we have,

$$\begin{aligned} \hat{\mathbf{u}} &= \mathbf{R}^{-1}\hat{\mathbf{v}}, \\ \dot{\hat{\mathbf{u}}} &= \frac{d}{dt^*}[\mathbf{R}^{-1}\hat{\mathbf{v}}] = \dot{\mathbf{R}}^{-1}\hat{\mathbf{v}} + \mathbf{R}^{-1}\dot{\hat{\mathbf{v}}}, \\ \ddot{\hat{\mathbf{u}}} &= \ddot{\mathbf{R}}^{-1}\hat{\mathbf{v}} + 2\dot{\mathbf{R}}^{-1}\dot{\hat{\mathbf{v}}} + \mathbf{R}^{-1}\ddot{\hat{\mathbf{v}}}. \end{aligned} \tag{2.2}$$

In vectorial notation the right hand side can be thought as,

$$\begin{aligned} -k^2\left(m_1\frac{\hat{\mathbf{u}} - \hat{\mathbf{u}}_{\mathbf{P1}}}{\hat{R}_1^3} + m_2\frac{\hat{\mathbf{u}} - \hat{\mathbf{u}}_{\mathbf{P2}}}{\hat{R}_2^3}\right) &= -k^2\left(m_1\frac{\mathbf{R}^{-1}\hat{\mathbf{v}} - \mathbf{R}^{-1}\hat{\mathbf{v}}_{\mathbf{P1}}}{\hat{R}_1^3} + m_2\frac{\mathbf{R}^{-1}\hat{\mathbf{v}} - \mathbf{R}^{-1}\hat{\mathbf{v}}_{\mathbf{P2}}}{\hat{R}_2^3}\right) = \\ &= -k^2\mathbf{R}^{-1}\left(m_1\frac{\hat{\mathbf{v}} - \hat{\mathbf{v}}_{\mathbf{P1}}}{\hat{R}_1^3} + m_2\frac{\hat{\mathbf{v}} - \hat{\mathbf{v}}_{\mathbf{P2}}}{\hat{R}_2^3}\right). \end{aligned}$$

Now we multiply the whole equation by $\mathbf{R}$. So we have to compute $\mathbf{S^1} = \mathbf{R}\dot{\mathbf{R}}^{-1}$ and $\mathbf{S^0} = \mathbf{R}\ddot{\mathbf{R}}^{-1}$. The results are,

$$\begin{aligned} \mathbf{S^1} &= \begin{pmatrix} 0 & -(n+\omega\cos i) & \omega\cos nt^*\sin i \\ n+\omega\cos i & 0 & -\omega\sin nt^*\sin i \\ -\omega\cos nt^*\sin i & \omega\sin nt^*\sin i & 0 \end{pmatrix}, \\ \mathbf{S^0} &= \begin{pmatrix} \mathbf{S^0_{1,1}} & \mathbf{S^0_{1,2}} & \mathbf{S^0_{1,3}} \\ \mathbf{S^0_{2,1}} & \mathbf{S^0_{2,2}} & \mathbf{S^0_{2,3}} \\ \mathbf{S^0_{3,1}} & \mathbf{S^0_{3,2}} & \mathbf{S^0_{3,3}} \end{pmatrix}, \\ \mathbf{S^0_{1,1}} &= -(n+\omega\cos i)^2 - \omega^2\cos^2 nt^*\sin^2 i, \\ \mathbf{S^0_{1,2}} &= \omega^2\sin nt^*\cos nt^*\sin^2 i, \\ \mathbf{S^0_{1,3}} &= \omega^2\sin nt^*\sin i\cos i, \\ \mathbf{S^0_{2,1}} &= \omega^2\sin nt^*\cos nt^*\sin^2 i, \\ \mathbf{S^0_{2,2}} &= -(n+\omega\cos i)^2 - \omega^2\sin^2 nt^*\sin^2 i, \\ \mathbf{S^0_{2,3}} &= \omega^2\cos nt^*\sin i\cos i, \\ \mathbf{S^0_{3,1}} &= \omega(2n+\omega\cos i)\sin nt^*\sin i, \\ \mathbf{S^0_{3,2}} &= \omega(2n+\omega\cos i)\cos nt^*\sin i, \\ \mathbf{S^0_{3,3}} &= -\omega^2\sin^2 i. \end{aligned}$$

Equations (2.1) become

$$\ddot{\hat{\mathbf{v}}} + 2\mathbf{S^1}\dot{\hat{\mathbf{v}}} + \mathbf{S^0}\hat{\mathbf{v}} = -k^2\left(m_1\frac{\hat{\mathbf{v}} - \hat{\mathbf{v}}_{\mathbf{P1}}}{\hat{r}_1^3} + m_2\frac{\hat{\mathbf{v}} - \hat{\mathbf{v}}_{\mathbf{P2}}}{\hat{r}_2^3}\right). \tag{2.3}$$

Since rotations preserve distances notice that $\hat{R}_1^3$ and $\hat{R}_2^3$ do not change. In any case we will change it by $\hat{r}_1^3$ and $\hat{r}_2^3$ respectively to indicate the distance from the third body to the primaries in the synodic frame.

Notice also that taking $i, \omega = 0$ the equations correspond to the usual RTBP since

$$\mathbf{S^1} = \begin{pmatrix} 0 & -n & 0 \\ n & 0 & 0 \\ 0 & 0 & 0 \end{pmatrix} \text{ and } \mathbf{S^0} = \begin{pmatrix} -n^2 & 0 & 0 \\ 0 & -n^2 & 0 \\ 0 & 0 & 0 \end{pmatrix}.$$

2.3 The GP-RTBP in dimensionless coordinates

At this point we are going to simplify the model taking dimensionless coordinates. The following changes are intended to do it:

$x = \dfrac{\hat{x}}{l}$, $y = \dfrac{\hat{y}}{l}$, $z = \dfrac{\hat{z}}{l}$, $r_1 = \dfrac{\hat{r}_1}{l}$, $r_2 = \dfrac{\hat{r}_2}{l}$, where $l = a + b$.

$\mu = \dfrac{m_2}{M}$, where $M = m_1 + m_2$, and therefore, $1 - \mu = \dfrac{m_1}{M}$.

From now on we can forget the hat over the variables, being XYZ and xyz the dimensionless sidereal and synodic frames. The coordinates of the primaries, like in the ordinary RTBP, are $\mathbf{v_{P1}} = (\mu, 0, 0)^T$ and $\mathbf{v_{P2}} = (\mu - 1, 0, 0)^T$.[2]

Introducing these changes equations (2.3) become

$$\ddot{\mathbf{v}} + 2\mathbf{S^1}\dot{\mathbf{v}} + \mathbf{S^0}\mathbf{v} = -n^2 \left((1-\mu)\frac{\mathbf{v} - \mathbf{v_{P1}}}{r_1^3} + \mu\frac{\mathbf{v} - \mathbf{v_{P2}}}{r_2^3} \right),$$

that is,

$$\begin{cases} \ddot{x} - 2(n + \omega\cos i)\dot{y} + 2\omega\cos nt^* \sin i\, \dot{z} &= [(n + \omega\cos i)^2 + \omega^2\cos^2 nt^* \sin^2 i]x \\ & \quad -\omega^2 \sin nt^* \cos nt^* \sin^2 i\, y \\ & \quad -\omega^2 \sin nt^* \sin i \cos i\, z \\ & \quad -n^2 \left[(1-\mu)\dfrac{x-\mu}{r_1^3} + \mu\dfrac{x-\mu+1}{r_2^3} \right], \\ \ddot{y} + 2(n + \omega\cos i)\dot{x} - 2\omega\sin nt^* \sin i\, \dot{z} &= -\omega^2 \sin nt^* \cos nt^* \sin^2 i\, x \\ & \quad +[(n + \omega\cos i)^2 + \omega^2 \sin^2 nt^* \sin^2 i]y \\ & \quad -\omega^2 \cos nt^* \sin i \cos i\, z \\ & \quad -n^2 \left[(1-\mu)\dfrac{y}{r_1^3} + \mu\dfrac{y}{r_2^3} \right], \\ \ddot{z} - 2\omega\cos nt^* \sin i\, \dot{x} + 2\omega\sin nt^* \sin i\, \dot{y} &= -\omega(2n + \omega\cos i)\sin nt^* \sin i\, x \\ & \quad -\omega(2n + \omega\cos i)\cos nt^* \sin i\, y \\ & \quad +\omega^2 \sin^2 i\, z - n^2 \left[(1-\mu)\dfrac{z}{r_1^3} + \mu\dfrac{z}{r_2^3} \right]. \end{cases}$$

[2] It can be seen from Kepler's Third Law that $\frac{b}{l} = \frac{m_2}{M} = \mu$ and $\frac{a}{l} = \frac{m_1}{M} = 1 - \mu$.

And if we prefer a first order ODE system:

$$\begin{cases} \dot{x}_1 &= x_4, \\ \dot{x}_2 &= x_5, \\ \dot{x}_3 &= x_6, \\ \dot{x}_4 &= 2(n+\omega\cos i)x_5 - 2\omega\cos nt^*\sin i\, x_6 + [(n+\omega\cos i)^2 + \omega^2\cos^2 nt^*\sin^2 i]x_1 \\ & \quad -\omega^2\sin nt^*\cos nt^*\sin^2 i\, x_2 - \omega^2\sin nt^*\sin i\cos i\, x_3 \\ & \quad -n^2\left[(1-\mu)\frac{x_1-\mu}{r_1^3} + \mu\frac{x_1-\mu+1}{r_2^3}\right], \\ \dot{x}_5 &= -2(n+\omega\cos i)x_4 + 2\omega\sin nt^*\sin i\, x_6 - \omega^2\sin nt^*\cos nt^*\sin^2 i\, x_1 \\ & \quad +[(n+\omega\cos i)^2 + \omega^2\sin^2 nt^*\sin^2 i]x_2 - \omega^2\cos nt^*\sin i\cos i\, x_3 \\ & \quad -n^2\left[(1-\mu)\frac{x_2}{r_1^3} + \mu\frac{x_2}{r_2^3}\right], \\ \dot{x}_6 &= 2\omega\cos nt^*\sin i\, x_4 - 2\omega\sin nt^*\sin i\, x_5 - \omega(2n+\omega\cos i)\sin nt^*\sin i\, x_1 \\ & \quad -\omega(2n+\omega\cos i)\cos nt^*\sin i\, x_2 + \omega^2\sin^2 i\, x_3 - n^2\left[(1-\mu)\frac{x_3}{r_1^3} + \mu\frac{x_3}{r_2^3}\right], \end{cases}$$

being $x_1 = x$, $x_2 = y$ and $x_3 = z$ [3].

Remark. Notice that we have maintained t^* in the equations to stress that the time is not a dimensionless variable. Here we could define $t = n\,t^*$ to make it dimensionless but we preferred to maintain it because the parameter n will be important in next sections. However, in most of the calculations we have taken $n = 1$ which is the same as taking the time dimensionless.

2.4 The GP-RTBP in a Hamiltonian form

In this section we want to compute the Hamiltonian of the system. First of all we compute the Lagrangian in sidereal coordinates. It is usually computed adding kinetic energy and negative potential. The potential in sidereal coordinates is

$$\mathcal{U}(X,Y,Z,t^*) \;=\; n^2\left(\frac{1-\mu}{R_1} + \frac{\mu}{R_2}\right).$$

Thus

$$\mathcal{L}(X,Y,Z,\dot{X},\dot{Y},\dot{Z},t^*) \;=\; \frac{1}{2}(\dot{X}^2+\dot{Y}^2+\dot{Z}^2) + \mathcal{U}(X,Y,Z,t^*).$$

The Lagrangian in synodic coordinates can be obtained using the transformation of coordinates (2.2) but taking into account that now is dimensionless, i.e.,

$$\begin{pmatrix}\dot{X}\\ \dot{Y}\\ \dot{Z}\end{pmatrix} \;=\; \dot{\mathbf{R}}^{-1}\begin{pmatrix}x\\ y\\ z\end{pmatrix} + \mathbf{R}^{-1}\begin{pmatrix}\dot{x}\\ \dot{y}\\ \dot{z}\end{pmatrix}.$$

[3] From now on, both notations, x_1, x_2, x_3 and x, y, z, will be indistinctly used.

The potential in synodic coordinates is

$$U(x,y,z) = n^2\left(\frac{1-\mu}{r_1}+\frac{\mu}{r_2}\right).$$

In consequence,

$$\begin{aligned} L(x,y,z,\dot{x},\dot{y},\dot{z},t^*) = & \frac{1}{2}[(n+\omega\cos i)^2+\omega^2\cos^2 nt^*\sin^2 i]x^2 \\ & +\frac{1}{2}[(n+\omega\cos i)^2+\omega^2\sin^2 nt^*\sin^2 i]y^2+\frac{1}{2}\omega^2\sin^2 i\ z^2 \\ & -\omega^2\sin nt^*\cos nt^*\sin^2 i\ xy-\omega(n+\omega\cos i)\sin nt^*\sin i\ xz \\ & +(n+\omega\cos i)x\dot{y}-\omega\cos nt^*\sin i\ x\dot{z} \\ & -\omega(n+\omega\cos i)\cos nt^*\sin i\ yz-(n+\omega\cos i)y\dot{x} \\ & +\omega\sin nt^*\sin i\ y\dot{z}+\omega\cos nt^*\sin i\ z\dot{x}-\omega\sin nt^*\sin i\ z\dot{y} \\ & +\frac{1}{2}[\dot{x}^2+\dot{y}^2+\dot{z}^2]+U(x,y,z). \end{aligned}$$

Now, we can use the Legendre transformation,

$$p_i=\frac{\partial L}{\partial\dot{q}^i}, \qquad\qquad H(q^i,p_i)=\sum_{i=1}^{n}p_i\dot{q}^i-L(q^i,p_i),$$

to obtain the momenta,

$$\begin{aligned} p_x &= \frac{\partial L}{\partial\dot{x}} = -(n+\omega\cos i)y+\omega\cos nt^*\sin i\ z+\dot{x}, \\ p_y &= \frac{\partial L}{\partial\dot{y}} = (n+\omega\cos i)x-\omega\sin nt^*\sin i\ z+\dot{y} \\ p_z &= \frac{\partial L}{\partial\dot{z}} = -\omega\cos nt^*\sin i\ x+\omega\sin nt^*\sin i\ y+\dot{z}, \end{aligned}$$

and the Hamiltonian,

$$\begin{aligned} H(x,y,z,p_x,p_y,p_z,t^*) = & \frac{1}{2}(p_x^2+p_y^2+p_z^2) \\ & -(n+\omega\cos i)xp_y+\omega\cos nt^*\sin i\ xp_z \\ & +(n+\omega\cos i)yp_x-\omega\sin nt^*\sin i\ yp_z \\ & -\omega\cos nt^*\sin i\ zp_x+\omega\sin nt^*\sin i\ zp_y \\ & -U(x,y,z). \end{aligned}$$

So the Hamiltonian equations are

$$\begin{cases} \dot{x} = (n+\omega\cos i)y-\omega\cos nt^*\sin i\ z+p_x, \\ \dot{y} = -(n+\omega\cos i)x+\omega\sin nt^*\sin i\ z+p_y, \\ \dot{z} = \omega\cos nt^*\sin i\ x-\omega\sin nt^*\sin i\ y+p_z, \\ \dot{p}_x = (n+\omega\cos i)p_y-\omega\cos nt^*\sin i\ p_z+U_x, \\ \dot{p}_y = -(n+\omega\cos i)p_x+\omega\sin nt^*\sin i\ p_z+U_y, \\ \dot{p}_z = \omega\cos nt^*\sin i\ p_x-\omega\sin nt^*\sin i\ p_y+U_z. \end{cases}$$

where

$$\begin{aligned} U_x &= -n^2\left[(1-\mu)\frac{x-\mu}{r_1^3}+\mu\frac{x-\mu+1}{r_2^3}\right], \\ U_y &= -n^2\left[(1-\mu)\frac{y}{r_1^3}+\mu\frac{y}{r_2^3}\right], \\ U_z &= -n^2\left[(1-\mu)\frac{z}{r_1^3}+\mu\frac{z}{r_2^3}\right]. \end{aligned}$$

Remark. Notice that if we consider a different potential the development is the same and equations only change in the terms corresponding to the partial derivatives of this potential.

2.5 Summary of equations of motion for GP-RTBP

The equations of motion in dimensionless sidereal coordinates are

$$\begin{cases} \dot{X}_1 = X_4, \\ \dot{X}_2 = X_5, \\ \dot{X}_3 = X_6, \\ \dot{X}_4 = -n^2\left[(1-\mu)\dfrac{(X_1-X_{P1})}{R_1^3}+\mu\dfrac{(X_1-X_{P2})}{R_2^3}\right], \\ \dot{X}_5 = -n^2\left[(1-\mu)\dfrac{(X_2-Y_{P1})}{R_1^3}+\mu\dfrac{(X_2-Y_{P2})}{R_2^3}\right], \\ \dot{X}_6 = -n^2\left[(1-\mu)\dfrac{(X_3-Z_{P1})}{R_1^3}+\mu\dfrac{(X_3-Z_{P2})}{R_2^3}\right], \end{cases}$$

where

$$\begin{aligned} R_1 &= \sqrt{(X_1-X_{P1})^2+(X_2-Y_{P1})^2+(X_3-Z_{P1})^2}, \\ R_2 &= \sqrt{(X_1-X_{P2})^2+(X_2-Y_{P2})^2+(X_3-Z_{P2})^2}, \\ X_{P1} &= \mu(\cos\omega t^*\cos nt^*-\sin\omega t^*\sin nt^*\cos i), \\ X_{P2} &= (\mu-1)(\cos\omega t^*\cos nt^*-\sin\omega t^*\sin nt^*\cos i), \\ Y_{P1} &= \mu(\sin\omega t^*\cos nt^*+\cos\omega t^*\sin nt^*\cos i), \\ Y_{P2} &= (\mu-1)(\sin\omega t^*\cos nt^*+\cos\omega t^*\sin nt^*\cos i), \\ Z_{P1} &= \mu\sin nt^*\sin i, \\ Z_{P2} &= (\mu-1)\sin nt^*\sin i. \end{aligned}$$

The equations of motion in dimensionless synodic coordinates are

$$\begin{cases} \dot{x}_1 &= x_4, \\ \dot{x}_2 &= x_5, \\ \dot{x}_3 &= x_6, \\ \dot{x}_4 &= 2ax_5 - 2b_2x_6 + [a^2 + b_2^2]x_1 - b_1b_2x_2 - b_1c_2x_3 \\ & \quad -n^2\left[(1-\mu)\frac{x_1-\mu}{r_1^3} + \mu\frac{x_1-\mu+1}{r_2^3}\right], \\ \dot{x}_5 &= -2ax_4 + 2b_1x_6 - b_1b_2x_1 + [a^2 + b_1^2]x_2 - b_2c_2x_3 - n^2\left[(1-\mu)\frac{x_2}{r_1^3} + \mu\frac{x_2}{r_2^3}\right], \\ \dot{x}_6 &= 2b_2x_4 - 2b_1x_5 - (n+a)b_1x_1 - (n+a)b_2x_2 + c_1^2x_3 - n^2\left[(1-\mu)\frac{x_3}{r_1^3} + \mu\frac{x_3}{r_2^3}\right], \end{cases}$$

where

$$\begin{aligned} a(n,\omega,i) = n + \omega\cos i, \quad & b_1(n,\omega,i,t^*) = \omega\sin nt^*\sin i, \quad c_1(\omega,i) = \omega\sin i, \\ & b_2(n,\omega,i,t^*) = \omega\cos nt^*\sin i, \quad c_2(\omega,i) = \omega\cos i, \end{aligned}$$

and

$$\begin{aligned} r_1 &= \sqrt{(x_1-\mu)^2 + x_2^2 + x_3^2}, \\ r_2 &= \sqrt{(x_1-\mu+1)^2 + x_2^2 + x_3^2}. \end{aligned}$$

In Hamiltonian form, we have

$$\begin{cases} \dot{x} &= ay - b_2z + p_x, \\ \dot{y} &= -ax + b_1z + p_y, \\ \dot{z} &= b_2x - b_1y + p_z, \\ \dot{p}_x &= ap_y - b_2p_z - n^2\left[(1-\mu)\frac{x-\mu}{r_1^3} + \mu\frac{x-\mu+1}{r_2^3}\right], \\ \dot{p}_y &= -ap_x + b_1p_z - n^2\left[(1-\mu)\frac{y}{r_1^3} + \mu\frac{y}{r_2^3}\right], \\ \dot{p}_z &= b_2p_x - b_1p_y - n^2\left[(1-\mu)\frac{z}{r_1^3} + \mu\frac{z}{r_2^3}\right]. \end{cases}$$

Remark. Remember that $X_1 = X$, $X_2 = Y$ and $X_3 = Z$, and similarly $x_1 = x$, $x_2 = y$ and $x_3 = z$. The transformation of coordinates between $\mathbf{u} = (X, Y, Z)^T$ and $\mathbf{v} = (x, y, z)^T$ is given by $\mathbf{u} = \mathbf{R}^{-1}\mathbf{v}$ and the momenta p_x, p_y and p_z are

$$p_x = -ay + b_2z + \dot{x},\ p_y = ax - b_1z + \dot{y} \text{ and } p_z = -b_2x + b_1y + \dot{z}.$$

3. Rigid body dynamics

In this section we consider a new model consisting in our two primaries joined by a fictitious massless bar which keeps the distance between them fixed. We will assume that exists an axis of symmetry. In rigid body dynamics, a body with this property is called a symmetric top.

3.1 General motion of a rigid body

With the purpose of explaining the most general possible motion of a symmetric top in a torque-free motion, this is, the motion of a body which has no forces acting on it, we are going to begin with some basic results in rigid body dynamics.

Let us consider a fixed coordinate system A in the space (space coordinates). Then, let us assume that there are several mass points m_i [4]. These points form a rigid body if distances between them remain constant. In vectorial form we say:

$$(\vec{r}_{A,i} - \vec{r}_{A,j})^2 = c_{i,j}$$

being $c_{i,j}$ a constant depending on the two mass points.

Now let us consider another coordinate system B with the origin in the centre of mass of the body (body coordinates). Let $\vec{r}_{B,i}$ be the position vector of a point of the body in B coordinates. The position vector in A coordinates is

$$\vec{r}_{A,i} = \vec{r}_{cm} + \vec{r}_{B,i}, \tag{3.1}$$

as shown in figure 3.1.

Notice that $\vec{r}_{cm} = \vec{r}_{A,cm}$ and $\vec{r}_{B,cm} = 0$. Denoting by $\vec{\omega}$ the angular velocity of the non-inertial frame with respect to the inertial and taking the derivative of (3.1) with respect to time we obtain

$$\vec{v}_{A,i} = \vec{v}_{cm} + \vec{\omega} \times \vec{r}_{B,i}. \tag{3.2}$$

Remark. Notice that in the expression above appears a term depending on $\vec{\omega}$. Remember that the derivatives of a vector $\vec{b}$ with respect to time in an inertial and non-inertial frame are related by

$$\left.\frac{d\vec{b}}{dt}\right|_S = \left.\frac{d\vec{b}}{dt}\right|_{S'} + \vec{\omega} \times \vec{b},$$

[4] The same discussion can be done if we think in a continuous distribution of mass. Nevertheless, it is easier to see firstly the whole discussion for point masses.

being S and S' the inertial and non-inertial frames respectively and $\vec{\omega}$ the angular velocity of the non-inertial frame with respect to the inertial.

The vector $\vec{r}_{B,i}$ has constant modulus, thus the only possible motion of the mass m_i with respect the centre of mass is a rotation of angular velocity $\vec{\omega}$ around an instantaneous axis that passes through the centre of mass. This allow us to decompose the motion of the body into two motions: the body motion with respect the space coordinates and the rotational motion of the body. Since we will use this theory to model our problem of two bodies, we are only interested in the rotational motion, ie, the motion of the bodies about the centre of mass.

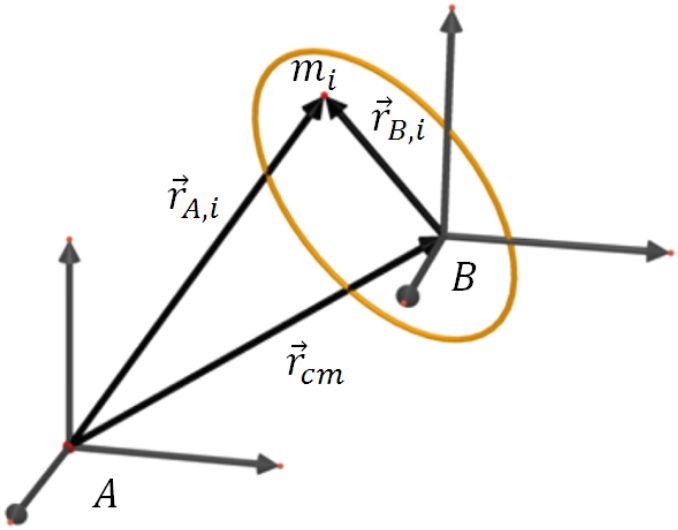

Figure 3.1. Relation between the two frames of reference.

The total kinetic energy in space coordinates is

$$T = \frac{1}{2}\sum_i m_i \vec{v}_{A,i}^2 = \frac{1}{2}\left(\sum_i m_i\right)\vec{v}_{cm}^2 + \vec{v}_{cm}\cdot\vec{\omega}\times\left(\sum_i m_i\vec{r}_{B,i}\right) + \frac{1}{2}\sum_i m_i\left(\vec{\omega}\times\vec{r}_{B,i}\right)^2$$

and notice that $\sum_i m_i = M$, the total mass, and $\sum_i m_i\vec{r}_{B,i} = M\vec{r}_{B,cm} = 0$. In this way the kinetic energy is the sum of two separate terms:

$$T = \frac{1}{2}\left(\sum_i m_i\right)\vec{v}_{cm}^2 + \frac{1}{2}\sum_i m_i\left(\vec{\omega}\times\vec{r}_{B,i}\right)^2 = T_{translation} + T_{rotation}.$$

In order to simplify the expressions and since we are only interested in the rotational part, we are going to avoid $\vec{r}_{B,i}$ notation and we will use, from now on, $\vec{r}_i$ to represent vectors in body coordinates. Using vector identities, it is not difficult to see[5] that the rotational part can be written as

$$T_{rotation} = \frac{1}{2}\sum_{\alpha,\beta}\omega_\alpha\omega_\beta I_{\alpha\beta},$$

[5]More details can be found in [11] and [12].

where α, $\beta = 1, 2, 3$ and

$$I_{\alpha\beta} = \sum_i m_i \left(r_i^2 \delta_{\alpha\beta} - r_{i,\alpha} r_{i,\beta} \right).$$

In this expression, $\delta_{\alpha\beta}$ is the Kronecker delta:

$$\delta_{\alpha\beta} = \begin{cases} 1, & \text{if} \quad \alpha = \beta \\ 0, & \text{if} \quad \alpha \neq \beta \end{cases}.$$

Using this, the rotational part of the kinetic energy can also be represented as

$$T_{rotation} = \frac{1}{2} \vec{\omega}^T \mathbf{I} \vec{\omega}$$

being $\mathbf{I}$ the moment of inertia tensor whose expression is

$$\mathbf{I} = \begin{pmatrix} \sum m_i(y_i^2 + z_i^2) & -\sum m_i x_i y_i & -\sum m_i x_i z_i \\ -\sum m_i x_i y_i & \sum m_i(x_i^2 + z_i^2) & -\sum m_i y_i z_i \\ -\sum m_i x_i z_i & -\sum m_i y_i z_i & \sum m_i(x_i^2 + y_i^2) \end{pmatrix}.$$

Remark. When the mass distribution is continuous, essentially we must replace the sum over mass points by a volume integral:

$$\mathbf{I} = \begin{pmatrix} \iiint \rho(y^2 + z^2)\, dx\, dy\, dz & -\iiint \rho xy\, dx\, dy\, dz & -\iiint \rho xz\, dx\, dy\, dz \\ -\iiint \rho xy\, dx\, dy\, dz & \iiint \rho(x^2 + z^2)\, dx\, dy\, dz & -\iiint \rho yz\, dx\, dy\, dz \\ -\iiint \rho xz\, dx\, dy\, dz & -\iiint \rho yz\, dx\, dy\, dz & \iiint \rho(x^2 + y^2)\, dx\, dy\, dz \end{pmatrix}$$

where $\rho(x, y, z)$ is the density function.

Since the inertia tensor is symmetric it is possible to find an orthogonal transformation $\mathbf{U}$ that diagonalizes $\mathbf{I}$:

$$\mathbf{U}\mathbf{I}\mathbf{U}^T = \begin{pmatrix} I_1 & 0 & 0 \\ 0 & I_2 & 0 \\ 0 & 0 & I_3 \end{pmatrix}.$$

Such coordinate axes are called the principal axes and the diagonal values are called the principal moments of inertia. Moreover, all the eigenvalues of the matrix are positive, so the kinetic energy will be always positive no matter what $\vec{\omega}$ is.

3.1.1 The angular momentum

When there are no torques applied, the angular momentum of a rigid body is preserved. In addition, there is a connection between angular momentum and angular velocity that we are going to show.

The total angular momentum of the system is defined by

$$\vec{L} = \sum_i m_i \left(\vec{r}_{A,i} \times \vec{v}_{A,i} \right).$$

Applying (3.1) and (3.2), and using the fact that we have centred the body coordinates in the centre of mass ($\sum_i m_i \vec{r}_i = 0$), we obtain

$$\vec{L} = \vec{r}_{cm} \times M\vec{v}_{cm} + \sum_i m_i \vec{r}_i \times (\vec{\omega} \times \vec{r}_i)\,.$$

Again we can see that total angular momentum is the sum of two: the part related to the motion of the centre of mass and a rotational part.

$$\vec{L} = \vec{L}_{translation} + \vec{L}_{rotation}.$$

And again, using vector identities, it is not difficult to see that

$$\vec{L}_{rotation} = \sum_\beta I_{\alpha\beta}\omega_\beta,$$

that is

$$\vec{L}_{rotation} = \mathbf{I}\vec{\omega}. \tag{3.3}$$

3.2 Euler equations for a torque-free motion

A body having no torques acting on it preserves its angular momentum. Therefore, its derivative with respect to time is null in space coordinates:

$$\left.\frac{d\vec{L}}{dt}\right|_A = 0.$$

In body coordinates, since the reference frame is non-inertial, time derivatives must be replaced by another expression that includes the fictitious forces associated to this non-inertiality:

$$\left.\frac{d\vec{L}}{dt}\right|_B + \vec{\omega} \times \vec{L} = 0. \tag{3.4}$$

Using (3.3) and the fact that the centre of mass position and velocity are null in body coordinates in equation (3.4), we get the Euler equations,

$$\begin{cases} I_1 \dfrac{d\omega_1}{dt} = \omega_3 L_2 - \omega_2 L_3 = \omega_2\omega_3\,(I_2 - I_3)\,, \\ I_2 \dfrac{d\omega_2}{dt} = \omega_1 L_3 - \omega_3 L_1 = \omega_1\omega_3\,(I_3 - I_1)\,, \\ I_3 \dfrac{d\omega_3}{dt} = \omega_2 L_1 - \omega_1 L_2 = \omega_1\omega_2\,(I_1 - I_2)\,. \end{cases}$$

3.3 Simple models with two connected spheres

Our model will consist in two spheres of radii a and b and masses M_1 and M_2 respectively. In order to apply the theory of rigid bodies, we are going to assume that both masses are connected by a massless bar. Figure 3.2 represents this model. Let us take the coordinate

system with origin at the centre of mass of the two spheres. In this way, the symmetry axis is denoted with the number 3 and the coordinates of the centres of the spheres are

$$M_1 = \left(0, 0, \frac{M_2 R}{M_1 + M_2}\right), \quad M_2 = \left(0, 0, \frac{-M_1 R}{M_1 + M_2}\right).$$

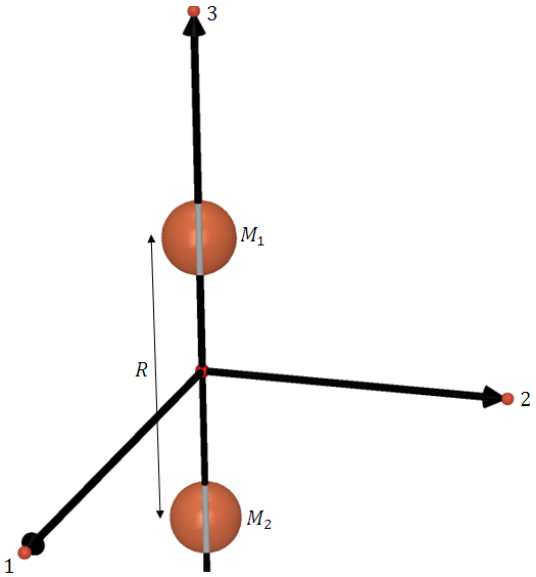

Figure 3.2. Representation of the model.

To compute the moment of inertia tensor of our rigid body, first we need to know the inertia tensor of a sphere with centre in the origin of the coordinate system. This can be computed using cylindrical coordinates. For a sphere of mass M, constant density ρ and radius a the principal moments of inertia are equal. Moreover, any axes that we could take are principal axes due to the symmetry of the sphere. Therefore

$$\mathbf{I} = \begin{pmatrix} I_1 & 0 & 0 \\ 0 & I_2 & 0 \\ 0 & 0 & I_3 \end{pmatrix}$$

where

$$I_1 = I_2 = I_3 = \int_{-a}^{a} \int_{0}^{2\pi} \int_{0}^{\sqrt{a^2 - z^2}} \rho r^2 r \, dr \, d\theta \, dz = \frac{8}{15} \rho \pi a^5.$$

We can think that the density of the sphere is

$$\rho = \frac{M}{\frac{4}{3}\pi a^3},$$

so

$$I_1 = I_2 = I_3 = \frac{2}{5} M_1 a^2.$$

Now, we can use the Displaced Axis Theorem to adapt this result to our case. This theorem states that if we know the moment of inertia tensor using the centre of mass

as the origin ($\mathbf{I}_{cm}$), and we wish to know the moment of inertia tensor about an origin displaced by $\vec{q}$, a constant vector, it is given by the formula,

$$\mathbf{I}_{\vec{q}} = \mathbf{I}_{cm} + M(q^2\delta_{\alpha\beta} - q_\alpha q_\beta).$$

In our case we take $\vec{q_1} = (0, 0, \frac{-M_2R}{M_1+M_2})$ and $\vec{q_2} = (0, 0, \frac{M_1R}{M_1+M_2})$ for spheres M_1 and M_2 respectively. For instance, to calculate I_2 for the sphere M_1 we do:

$$I_2 = \frac{2}{5}M_1a^2 + M_1q^2 = \frac{2}{5}M_1a^2 + M_1\left(\frac{M_2R}{M_1+M_2}\right)^2.$$

Then adding the results of both spheres, we obtain the moment of inertia tensor of our model:

$$\mathbf{I} = \begin{pmatrix} I_1 & 0 & 0 \\ 0 & I_2 & 0 \\ 0 & 0 & I_3 \end{pmatrix}$$

where

$$\begin{aligned} I_1 &= \frac{2}{5}M_1a^2 + M_1\left(\frac{M_2R}{M_1+M_2}\right)^2 + \frac{2}{5}M_2b^2 + M_2\left(\frac{M_1R}{M_1+M_2}\right)^2, \\ I_2 &= \frac{2}{5}M_1a^2 + M_1\left(\frac{M_2R}{M_1+M_2}\right)^2 + \frac{2}{5}M_2b^2 + M_2\left(\frac{M_1R}{M_1+M_2}\right)^2, \\ I_3 &= \frac{2}{5}M_1a^2 + \frac{2}{5}M_2b^2. \end{aligned} \tag{3.5}$$

Notice that, as we previously said, our body is a symmetric top since $I_1 = I_2 \neq I_3$. There exists two types of symmetric tops. It depends on $I_1 = I_2 > I_3$ (prolate case) or $I_1 = I_2 < I_3$ (oblate case). From (3.5) we are in the prolate case. Therefore, Euler equations are

$$\begin{cases} \dfrac{d\omega_1}{dt} = -\omega_2\omega_3\left(\dfrac{I_3}{I_1} - 1\right), \\ \dfrac{d\omega_2}{dt} = \omega_1\omega_3\left(\dfrac{I_3}{I_1} - 1\right), \\ \dfrac{d\omega_3}{dt} = 0. \end{cases} \tag{3.6}$$

Then, ω_3 must be constant. Let us define $\Omega_p = \omega_3\left(\dfrac{I_3}{I_1} - 1\right)$. Combining the two equations of (3.6) that are not trivial we have as a result

$$\frac{d^2\omega_1}{dt^2} = -\Omega_p^2\omega_1, \quad \frac{d^2\omega_2}{dt^2} = -\Omega_p^2\omega_2.$$

The solution of these equations are

$$\omega_1(t) = -A\sin(\Omega_p t) + B\cos(\Omega_p t), \quad \omega_2(t) = A\cos(\Omega_p t) + B\sin(\Omega_p t).$$

Since the third component of the angular velocity is constant but not the others, this vector precesses around the symmetry axis 3.

In this way, we can compute the angular momentum, $\vec{L}$, using (3.3):

$$\vec{L} = \mathbf{I}\vec{\omega} = \begin{pmatrix} I_1\left(-A\sin\left(\Omega_p t\right) + B\cos\left(\Omega_p t\right)\right) \\ I_2\left(A\cos\left(\Omega_p t\right) + B\sin\left(\Omega_p t\right)\right) \\ I_3\omega_3 \end{pmatrix}.$$

Notice that $\vec{L}$ is not constat. This is because it must be constant in space coordinates and the expression above refers to body coordinates.

Now we are going to find what are the values of A, B and ω_3. Suppose that space coordinates have their third axis, Z', in the direction of the constant vector $\vec{L}$ and suppose also that the third axis of the body coordinates, 3, is tilted at an angle θ from Z'. When $t = 0$, imagine that the planes $Y'Z'$ and 23 are the same.

If we define Ω to be the angular velocity of the body around its third axis, then, it can be seen that

$$\vec{\omega} = \begin{pmatrix} 0 \\ 0 \\ \Omega \end{pmatrix} + \vec{\omega}_p$$

where $\vec{\omega_p}$ is the missing part of the angular velocity, and $\omega_p = \dfrac{L}{I_1}$. Following the discussion in [12] we obtain

$$A = \frac{L}{I_1}\sin(\theta)\,, \quad B = 0 \quad \text{and} \quad \omega_3 = \frac{L}{I_3}\cos(\theta).$$

Therefore,

$$\vec{\omega} = \begin{pmatrix} -\dfrac{L}{I_1}\sin(\theta)\sin\left(\Omega_p t\right) \\ \dfrac{L}{I_1}\sin(\theta)\cos\left(\Omega_p t\right) \\ \dfrac{L}{I_3}\cos(\theta) \end{pmatrix} \tag{3.7}$$

It is easy to check that $\Omega = -\Omega_p$.

3.3.1 Angular velocity in terms of Euler angles

It can be proved that angular velocity in body coordinates has the expression

$$\vec{\omega} = \begin{pmatrix} \dot{\theta}\cos(\psi) + \dot{\phi}\sin(\psi)\sin(\theta) \\ -\dot{\theta}\sin(\psi) + \dot{\phi}\cos(\psi)\sin(\theta) \\ \dot{\psi} + \dot{\phi}\cos(\theta) \end{pmatrix}.$$

ψ is the angle related to the rotation of the body, ϕ to the precession and θ to the nutation.

From the expression above and (3.7),

$$\begin{array}{lll} \phi = \omega_p t, & \theta = \text{constant}, & \psi = \Omega t, \\ \dot{\phi} = \omega_p, & \dot{\theta} = 0, & \dot{\psi} = \Omega. \end{array} \tag{3.8}$$

Once we know the Euler angles, we can build matrix **R** (or its inverse) which is the change of coordinates from body coordinates to space coordinates.

Remark. In the matrix **R** (in fact, its inverse) we will switch columns to put the masses into the first axis of body coordinates, so this is more natural to compare the results between this model and the previous one.

We realize that the motion of primary bodies is not like we wanted unless $\theta = \frac{\pi}{2}$. This makes that the axis of symmetry of the body, which firstly is the third but then the first, is perpendicular to the angular momentum $\vec{L}$, defined from the beginning in the direction of the third axis of space coordinates.

3.3.2 A model with applied torque

Figure 3.3 shows what would be the motion of the primaries in this new model if there is not any torque applied to the body formed by the spheres.

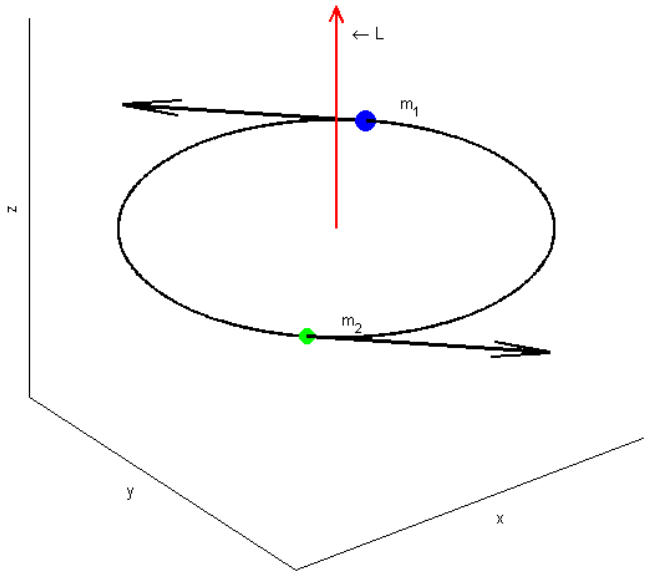

Figure 3.3. Motion of the primaries when $\theta = \frac{\pi}{2}$ (sidereal frame of reference).

This is, like the primaries in the RTBP, describing a circumference. So torque-free motion of this body does not seem to be like we wanted. Therefore, we have to introduce some changes in order make the plane containing the trajectory precess. The first thing someone could think is to take Euler angles in a way to eliminate the rotation ($\psi = 0$) and to make precess the body $\left(\theta = \frac{\pi}{2} + \alpha \sin(\beta t)\right)$. Actually, it is not a precession because we are changing the angle related to nutation phenomenon (the movement that varies the axis of rotation of a body). However, this change is what produces the movement that we are thinking of (figure 3.4). Notice that these expressions of the Euler angles do not have to make the body satisfy the Euler equations.

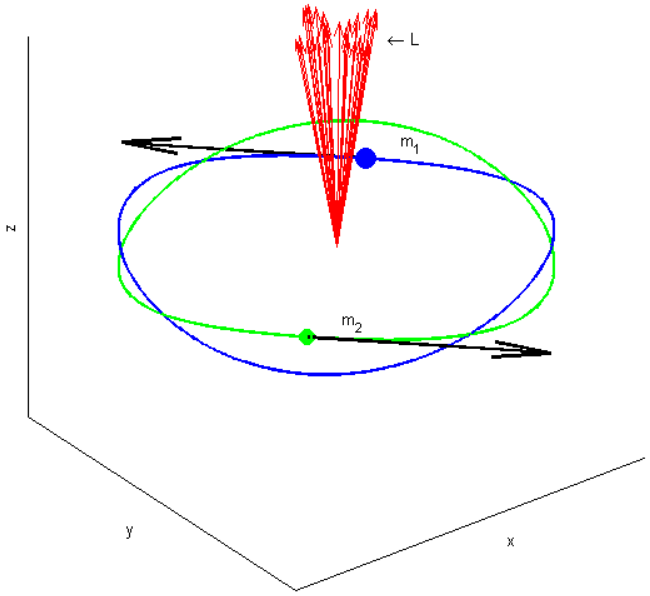

Figure 3.4. Motion of the primaries when $\theta = \frac{\pi}{2} + \alpha \sin(\beta t)$ (sidereal frame of reference). Red arrows indicate some of the angular momenta of the body as it revolves.

The parameter α represents the maximum tilt that a sphere can achieve respect plane $z = 0$ and β the oscillation frequency. The motion of primaries is determined by $\mathbf{R}$ and only depends on three values: ω_p, α and β. In sidereal coordinates:

$$\vec{p}_1 = \mu \begin{pmatrix} \cos(\omega_p t)\cos(\alpha \sin(\beta t)) \\ \sin(\omega_p t)\cos(\alpha \sin(\beta t)) \\ -\sin(\alpha \sin(\beta t)) \end{pmatrix}, \quad \vec{p}_2 = (\mu - 1) \begin{pmatrix} \cos(\omega_p t)\cos(\alpha \sin(\beta t)) \\ \sin(\omega_p t)\cos(\alpha \sin(\beta t)) \\ -\sin(\alpha \sin(\beta t)) \end{pmatrix}$$

Following a similar discussion like we did in the first model we obtain the equations of this particular RTBP[6]:

$$\begin{cases} \dot{x}_1 &= x_4, \\ \dot{x}_2 &= x_5, \\ \dot{x}_3 &= x_6, \\ \dot{x}_4 &= 2\,n\,a_2\,x_5 - 2\,b\,x_6 + (n^2\,a_2^2 + b^2)\,x_1 + (n^2\,a_1\,a_2 - \dot{b})\,x_3 \\ & \quad -n^2 \left[(1-\mu)\frac{x_1 - \mu}{r_1^3} + \mu \frac{x_1 - \mu + 1}{r_2^3} \right], \\ \dot{x}_5 &= -2\,n\,a_2\,x_4 - 2\,n\,a_1\,x_6 + 2\,n\,a_1\,b\,x_1 + n^2\,x_2 - 2\,n\,a_2\,b\,x_3 - n^2 \left[(1-\mu)\frac{x_2}{r_1^3} + \mu \frac{x_2}{r_2^3} \right], \\ \dot{x}_6 &= 2\,b\,x_4 + 2\,n\,a_1\,x_5 + (n^2\,a_1\,a_2 + \dot{b})\,x_1 + (n^2\,a_1^2 + b^2)\,x_3 - n^2 \left[(1-\mu)\frac{x_3}{r_1^3} + \mu \frac{x_3}{r_2^3} \right]. \end{cases}$$

being

$$\begin{aligned} a_1 &= \sin(\varepsilon), \quad b = \dot{\varepsilon}, \quad \varepsilon = \alpha \sin(\beta t), \\ a_2 &= \cos(\varepsilon). \end{aligned}$$

[6]Since ω_p represents the mean motion of the primaries, we redefine ω_p as n.

In next sections we will refer to this model as Rigid Body with Applied Torque RTBP (RBAT-RTBP) or simply model 2. Although this model is correct, it has an inconvenience. We are considering an external force to cause the torque and we do not know exactly how this force is related to the factors which cause it. This force arises from taking the Euler angles as above and not respecting the Euler equations for a torque-free motion of a symmetric top. In order to obtain a compact model it would be better to consider a torque-free model.

3.3.3 A torque-free motion model

Having made all the calculations for the model of two spheres connected by a massless bar which considers an external force is very advantageous. The profit lies in the Euler angles we took. The nutation angle was $\theta = \frac{\pi}{2} + \varepsilon$ being $\varepsilon = \alpha \sin(\beta t)$. Remember that when α is null, $\theta = \frac{\pi}{2}$ and the motion is purely circular as in the RTBP.

From (3.8) we know that θ must be constant unlike the model previously considered. However, it must be different from $\frac{\pi}{2}$. Since the precession we are looking for seems to be controlled by a parameter which takes near-to-zero values, we realize that $\theta = \frac{\pi}{2} + \varepsilon$ where ε is any small negative constant value may cause the desired motion. So the calculations we did before will be useful in this case. We only have to take into account that ε is constant and then $\dot{\varepsilon} = 0$.

Remark. Notice that $\theta = \frac{\pi}{2} + \varepsilon$. For this reason ε will take small negative values since we want the bar to have an inclination $\theta \leq \frac{\pi}{2}$.

ϕ will remain as nt to cause the translation of the primaries around its centre of mass with mean motion n. ψ can be taken as null. Since ψ is the angle related to the rotation of the body, i.e., the rotation of the body around its axis of symmetry, it does not matter at all the velocity we take for it because this will not affect to the motion of a third body. In principle, its expression should be $\psi = \Omega t$ being $\Omega = \frac{L}{I_3}\cos(\theta)\left(1 - \frac{I_3}{I_1}\right)$, which is not null if $\theta = \frac{\pi}{2} + \varepsilon$. Comparing these two situations we consider two trajectories integrated from the same initial condition, the first with the right value of ψ with respect to the Euler equations of torque-free motion and the second taking ψ null. In fact, these two trajectories are different compared in its respective body coordinates but once changed into space coordinates they represent the same trajectory. So, strictly speaking, taking $\psi = 0$ entails an applied torque to the body. In spite of this, this torque does not affect to the motion of the third body in which we are interested. Figure 3.5 represents the motion of the primaries in this case. From now on, this model will be called Rigid Body Torque-Free RTBP (RBTF-RTBP) or model 3.

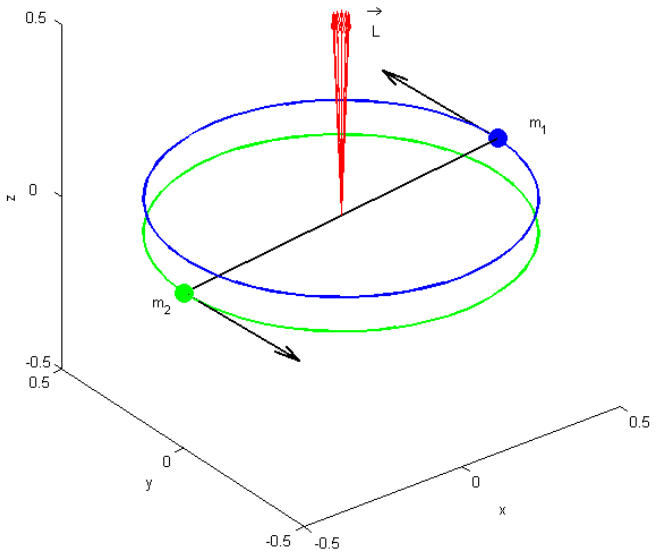

Figure 3.5. Motion of the primaries in the RBTF-RTBP (sidereal frame of reference). Red arrows indicate some of the angular momenta of the body as it revolves.

The equations of motion of model 3 are:

$$\begin{cases} \dot{x}_1 &= x_4, \\ \dot{x}_2 &= x_5, \\ \dot{x}_3 &= x_6, \\ \dot{x}_4 &= 2\,n\,\cos(\varepsilon)\,x_5 + n^2\,\cos(\varepsilon)^2\,x_1 + n^2\,\sin(\varepsilon)\,\cos(\varepsilon)\,x_3 \\ &\quad -n^2\left[(1-\mu)\dfrac{x_1-\mu}{r_1^3} + \mu\dfrac{x_1-\mu+1}{r_2^3}\right], \\ \dot{x}_5 &= -2\,n\,\cos(\varepsilon)\,x_4 - 2\,n\,\sin(\varepsilon)\,x_6 + n^2\,x_2 - n^2\left[(1-\mu)\dfrac{x_2}{r_1^3} + \mu\dfrac{x_2}{r_2^3}\right], \\ \dot{x}_6 &= 2\,n\,\sin(\varepsilon)\,x_5 + n^2\,\sin(\varepsilon)\,\cos(\varepsilon)\,x_1 + n^2\,\sin(\varepsilon)^2\,x_3 - n^2\left[(1-\mu)\dfrac{x_3}{r_1^3} + \mu\dfrac{x_3}{r_2^3}\right], \end{cases}$$

and it is important to emphasise that this is an autonomous system. As a consequence, like in the RTBP, there will be critical points and we will compute it afterwards.

Following the same procedure like that we did in the first model, the Hamiltonian can be computed from the Lagrangian:

$$\begin{aligned} H(x_1,x_2,x_3,x_4,x_5,x_6) &= \frac{1}{2}\left(x_4^2+x_5^2+x_6^2\right) - n^2\,\sin(\varepsilon)\,\cos(\varepsilon)\,x_1\,x_3 \\ &\quad -\frac{1}{2}\left(n^2\,\cos^2(\varepsilon)\,x_1^2 + n^2\,x_2^2 + n^2\,\sin^2(\varepsilon)\,x_3^2\right) - U\left(x_1,x_2,x_3\right). \end{aligned}$$

Remember that $U(x_1,x_2,x_3) = n^2\left[\frac{1-\mu}{r_1}+\frac{\mu}{r_2}\right]$ is the potential caused by the two bodies we are considering. The fact that now they are spheres instead of point masses is not

relevant in the potential as it is in the discussion of the motion of the whole body.

Proceeding as in the RTBP, the equations of motion admit of a Jacobi constant,

$$\begin{aligned} C(x_1, x_2, x_3, x_4, x_5, x_6) &= -\left(x_4^2 + x_5^2 + x_6^2\right) + 2n^2 \sin(\varepsilon)\cos(\varepsilon)\, x_1\, x_3 \\ &\quad + n^2 \cos^2(\varepsilon)\, x_1^2 + n^2\, x_2^2 + n^2 \sin^2(\varepsilon)\, x_3^2 + 2U, \end{aligned}$$

and, as usual, $C = -2H$.

An important thing to highlight is the absence of the time variable, t, in this constant of motion. This will allow us to compute the zero-velocity curves or, more generally, the zero-velocity surfaces which delimit the regions where the third body is allowed to move on.

3.4 An application to galactic dynamics

In previous sections we have been dealing with simple models, some of them unrealistic, but they have helped us to gain an insight into the matter. Using all the work that we have done until now, we will try to apply some of the developed tools to the galactic dynamics. We will focus our efforts in barred galaxy models, assuming that the bar behaves like a rigid body. Particularly, we will study the invariant objects which causes the formation of the spiral arms in [15] and how they are affected by inflicting a precession to the bar.

One of the models most used in galactic dynamics and the one we are going to study is the Miyamoto-Nagai Ferrers. However, the implementation to other galactic models is equally straightforward. These models have equations very similar with respect to the RTBP. The main difference is the fact that now we are not considering two masses describing circles but a bar. The body that revolves (two masses, a bar,...) affects the equations in the part corresponding to the potential. So now we have to focus in the components of the orbital structure of barred galaxies: a bar, a disc and sometimes a bulge. In [15] the author describes thoroughly some other possible potentials to be considered, this is, the bar potentials (Ferrers, BW, Dehnen and Logarithmic), the bulge potential and the disc potentials (Kuzmin-Toomre and Miyamoto-Nagai). Then, the potential of a galactic model of this type is divided into three components: $U = U_1 + U_2 + U_3$, each one of them corresponding to the bar, the disc and the bulge respectively.

In order to cause the precession, let us take model 3 in which two spheres connected with a massless bar moved as a rigid body with no torques applied on it. Remember that the discussions we did with models 1, 2 and 3 were independent of the potential we took then. This entails an important advantage: we can follow the same procedure but adapting the potential to our new situation. The potential part of the equations is related to the spheres so this part has to be replaced with a potential which considers the components of the barred galaxy. We assume that the barred galaxies we want to study have a bar and a disc but do not have bulge. With precession, the bar and the disc will be tilted a small angle ε in sidereal coordinates (figure 3.6). However,

in the synodic frame of reference, the bar is fixed in the x axis and the disc is embedded in the plane $z = 0$. So the resultant potential of the galactic model, U, will be the sum of two components, $U = U_1 + U_2$, where U_1 will be the Ferrers bar potential and U_2 the Miyamoto-Nagai disc potential. The main advantage of this model is that the system of equations is autonomous.

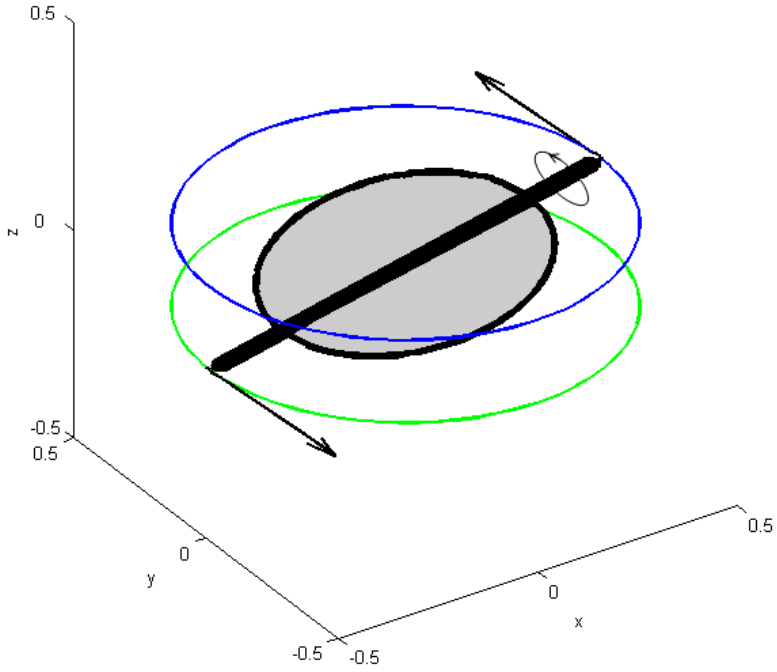

Figure 3.6. Motion of the bar and the disc in the sidereal frame of reference. In addition to the precession, the bar revolves around its symmetry axis (torque-free motion).

Here we present the expressions of Ferrers and Miyamoto-Nagai potentials:

$$U_1 = \pi\, G\, a_b\, b_b\, c_b\, \frac{\rho_0}{n+1} \int_\lambda^\infty \frac{du}{\Delta(u)} (1 - m^2(u))^{(n_h+1)},$$

$$U_2 = -\frac{Gm_d}{\sqrt{R^2 + (a_d + \sqrt{b_d^2 + z^2})^2}}.$$

On the one hand, a_b, b_b and c_b are the semiaxes of an ellipsoid, G the gravitational constant, n_h the homogeneity degree, ρ_0 the density at the origin,

$$\Delta(u) = (a_b^2 + u)(b_b^2 + u)(c_b^2 + u),$$

$$m^2(u) = \frac{x^2}{a_b^2 + u} + \frac{y^2}{b_b^2 + u} + \frac{z^2}{c_b^2 + u}$$

and λ the unique positive solution of $m^2(\lambda) = 1$ if $m^2(0) \geq 1$ and zero, otherwise. On the other hand, $R^2 = x^2 + y^2$ is the radius, a_d and b_d are the semiaxes and m_d the mass of

the disc.

Summarising all the explained above and considering all the assumptions we made in model 3, the following equations describe the motion of the Precessing Miyamoto-Nagai Ferrers galactic model.

$$\begin{cases} \dot{x}_1 &= x_4, \\ \dot{x}_2 &= x_5, \\ \dot{x}_3 &= x_6, \\ \dot{x}_4 &= 2\,n\,\cos(\varepsilon)\,x_5 + n^2\,\cos(\varepsilon)^2\,x_1 + n^2\,\sin(\varepsilon)\,\cos(\varepsilon)\,x_3 + U_{x_1}, \\ \dot{x}_5 &= -2\,n\,\cos(\varepsilon)\,x_4 - 2\,n\,\sin(\varepsilon)\,x_6 + n^2\,x_2 + U_{x_2}, \\ \dot{x}_6 &= 2\,n\,\sin(\varepsilon)\,x_5 + n^2\,\sin(\varepsilon)\,\cos(\varepsilon)\,x_1 + n^2\,\sin(\varepsilon)^2\,x_3 + U_{x_3}, \end{cases}$$

being ε the tilt angle and n the angular velocity of the bar[7]. Moreover, the potential U is decomposed as follows:

$$U = U_1 + U_2.$$

Remark. The derivatives of the Ferrers potential are not trivial. The case considered in this work is $n_h = 2$. Further information about the Ferrers potential can be found in [10].

[7]Although the bar is now an ellipsoid, it moves like the two spheres connected, so n is like the mean motion if we think that the spheres are located at the ends of the bar.

4. Numerical studies

The calculations of this chapter have been made by means of ad hoc routines and programmes under FORTRAN language. First we present some results of the GP-RTBP. Then, some results of the models considering rigid body dynamics are presented. In the first place the model in which there is an applied torque (RBAT-RTBP) and then the torque-free model (RBTF-RTBP). Finally we expose some results of the Precessing Miyamoto-Nagai Ferrers galactic model. Most of the computations are related to the critical points of the RTBP because some of the analysed periodic orbits reside near these points when the parameters which influence the models take small values. For simplicity we will restrict our computations to the L_2 point though all the procedures used can be adapted to other critical points.

4.1 The Giroscopically Precessing RTBP

Our first model consisted in a modification of the RTBP considering three parameters: the precession velocity, ω, the tilt angle, i and the mean motion of the primaries, n. In order to simplify the model and because we only want to know how the precession velocity and the tilt influence the motion, we thought to define $n = 1$. One thing to be considered in this model is the degenerate case when $i = 0$. In that case, the precession velocity continues existing and influencing the equations as we can see in section 2.5. Then, the whole system could be thought as a RTBP being the mean motion of the primaries $n+\omega$. So, although the model is simple, which is and advantage, this behaviour in the degenerate case is not what we want. This is the principal reason to consider other models in the present work. However, we present the analysis around the periodic orbits of this model because it will be useful in the other models.

First of all, the analysis is focused on seeing how the critical points existing in the RTBP change due to the precession phenomenon. They are replaced by periodic orbits which we want to compute. The procedure explained below is the chosen to achieve this objective. Then, we see how the parameters of the model affect the shape of these periodic orbits.

4.1.1 The parallel shooting method

In this section we are going to explain the parallel shooting method intended to find some periodic orbits in a Hamiltonian system.

Let $x_0 \in \mathbb{R}^n$ be the initial condition of the periodic orbit, T the period and $\Phi_t(x)$ the point after integrating x t units of time.

In order to obtain a periodic orbit, we want to solve

$$\Phi_T(x_0) - x_0 = 0.$$

However the periodic orbit may be unstable. This is, if we integrate T units of time the initial condition of a periodic orbit, the final point will not match the first one due to the numerical integration. To avoid this problem, we will consider k points on the periodic orbit $(x_0, x_1, \ldots, x_{k-1})$ and $\delta = \frac{T}{k}$. Then, the method consists in solving the following equations:

$$\begin{cases} \Phi_\delta(x_0) - x_1 = 0, \\ \vdots \\ \Phi_\delta(x_{k-2}) - x_{k-1} = 0, \\ \Phi_\delta(x_{k-1}) - x_0 = 0. \end{cases}$$

The idea is the following: instead of integrating T units of time, which entails unstability, we break the orbit in k pieces. Each one must begin in the end point of the previous and finish in the start point of the next. The advantage is that now we only have to integrate each point δ units of time. In this way the unstability is considerably reduced.

So we have a system of $n \times k$ equations and $n \times k$ unknowns. If we call $X = (x_0, x_1, \ldots, x_{k-1})$ and

$$F(X) = \begin{cases} \Phi_\delta(x_0) - x_1, \\ \vdots \\ \Phi_\delta(x_{k-2}) - x_{k-1}, \\ \Phi_\delta(x_{k-1}) - x_0, \end{cases}$$

we can solve the system $F(X) = 0$ by means of the Newton method. Therefore, it is necessary to obtain $DF(X)$:

$$DF(X) = \begin{pmatrix} D\Phi_\delta(x_0) & -Id & \mathbf{0} & \ldots & \mathbf{0} & \mathbf{0} \\ \mathbf{0} & D\Phi_\delta(x_1) & -Id & \ldots & \mathbf{0} & \mathbf{0} \\ \mathbf{0} & \mathbf{0} & D\Phi_\delta(x_2) & \ldots & \mathbf{0} & \mathbf{0} \\ \vdots & \vdots & \vdots & \ddots & \vdots & \vdots \\ \mathbf{0} & \mathbf{0} & \mathbf{0} & \ldots & D\Phi_\delta(x_{k-2}) & -Id \\ -Id & \mathbf{0} & \mathbf{0} & \ldots & \mathbf{0} & D\Phi_\delta(x_{k-1}) \end{pmatrix}$$

where Id is the $n \times n$ identity matrix. Then, the Newton method stands

$$DF(X^r)\Delta X^r = -F(X^r), \quad X^{r+1} = X^r + \Delta X^r, \quad r \geq 0.$$

4.1.2 Dynamical substitutes of critical points

We are going to find some periodic orbits substituting the L_2 libration point of the RTBP using the procedure explained above.

First of all, we need an initial condition. We will use the coordinates of the libration point, i.e., if the L_2 point of the RTBP has coordinates $L_2 = (l_2, 0, 0, 0, 0, 0)$ then,

we will take $X^0 = (x_0, \ldots, x_{k-1}) = (L_2, \ldots, L_2)$, this is, $x_0, x_1, \ldots, x_{k-1} = L_2$. We take all the points being the same because for a small values of ω and i we suspect that the periodic orbit created instead of L_2 is very close to this point.

After few iterations of the Newton method we have:

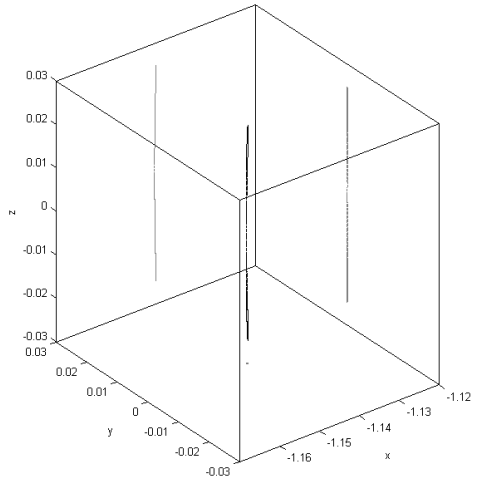

Figure 4.1. Periodic orbit substituting L_2 libration point and its projections obtained for the values $\omega = 0.1$ and $i = 0.1$.

It was enough to take $k = 5$ in the parallel shooting method to avoid the problems with the unstable behaviour of the orbit.

Since it is difficult from figure 4.1 to appreciate what is the shape of the orbit, figure 4.2 shows the same orbit but in this case the units are different depending on the axis.

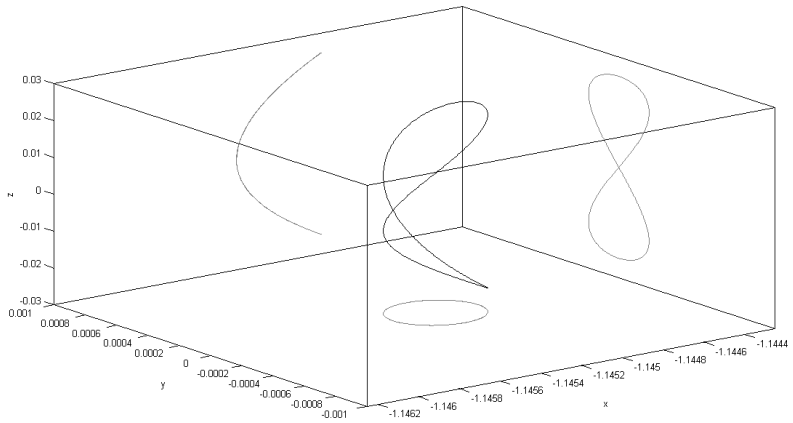

Figure 4.2. Orbit from figure 4.1 but changing the scale of the axes.

4.1.3 Continuation procedure

Now the objective consists in figuring out how the shape of the orbits depends on the parameters ω and i.

Firstly we will take $\omega = 0.1$. Then, varying i in the range $[0, 0.3]$ and computing the orbits will allow us to see the changes (figure 4.3).

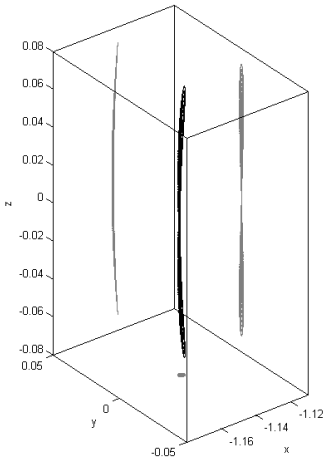

Figure 4.3. Family of periodic orbits fixing $\omega = 0.1$ and $i \in [0, 0.3]$.

Now we do the same but fixing $i = 0.1$ and $\omega \in [0, 0.3]$ (figure 4.4).

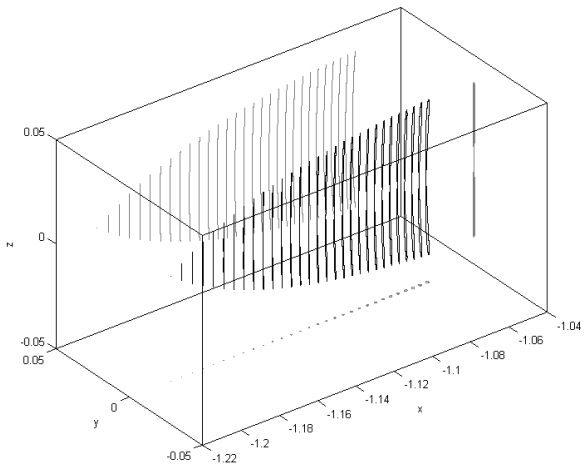

Figure 4.4. Family of periodic orbits fixing $i = 0.1$ and $\omega \in [0, 0.3]$.

A problem arises when we realize that for some values of ω and i, the parallel shooting method does not converge. We suspect that there are some regions in the plane of parameters $\omega - i$ where the method is unable to find the periodic orbits. To get an idea

of the situation, it will be only necessary to use values of ω and i in the interval $[0, 1]$. Moreover, the parameter i is 2π-periodic but we will not use inclinations greater than $\frac{\pi}{4} \simeq 0.785$.

The first thing to do is to take a grid of points in the square $[0, 1] \times [0, 1]$ and see if the method converges at each point. For simplicity, we use equidistant points in both directions with distance 10^{-3}: $\omega_0 = 0$, $\omega_1 = 0.001$,... and the same for i. We begin computing the periodic orbit with $(\omega_0, i_0) = (0, 0)$, so we are in the RTBP. Then $(0, 0.001)$, $(0, 0.002)$ and so on...

The initial condition for the method we have to take at each point will be computed from the previous ones using linear interpolation. For example, assume that we have fixed $\omega = \omega_r$ and we know a good initial condition for (ω_r, i_{s-2}) and (ω_r, i_{s-1}), i.e., we know that $X_{s-2} = (x_0^{s-2}, \ldots, x_k^{s-2})$ and $X_{s-1} = (x_0^{s-1}, \ldots, x_k^{s-1})$ are points of their respective periodic orbits. Then, using linear interpolation in the direction of i, we will take as initial condition for the method

$$X_s = ai_s + b$$

where

$$a = \frac{X_{s-1} - X_{s-2}}{i_{s-1} - i_{s-2}}$$

and

$$b = X_{s-2} - ai_{s-2} = X_{s-1} - ai_{s-1}.$$

This is for $s \geq 2$. If $s < 2$ we take the coordinates of the libration point as initial condition because the parameters are almost null.

Another problem we have to face in this procedure to compute "the map of periodic orbits" is the determination of a proper initial condition. Sometimes it is not possible to determine if the method converges to a certain point because the points used to compute the initial condition could make the method diverge. In that case, which are the best points to use in the determination of the initial condition of the Newton method?

As means of solving this problem we add some modifications to the program. Basically we start computing the map of a grid of distance 10^{-1} among its points, using the same system as before. Then, we save in a file all this periodic orbits and start computing the periodic orbits for a grid of distance 10^{-2}. This time, when we want to find an initial condition for each point in the parameter field, we do a search in the file to find the nearest periodic orbit we have obtained in the previous step and use it. The problem now is that for a given point in which a periodic orbit exists, its nearest periodic orbit in the file could be far enough to make the method diverge. This could be avoided adding the new periodic orbits to the file and starting again the program for the same grid until there are not new periodic orbits found.

In the final step we compute the map for a grid of distance 10^{-3} among its points. This calculation takes a lot of time so it is done only once.

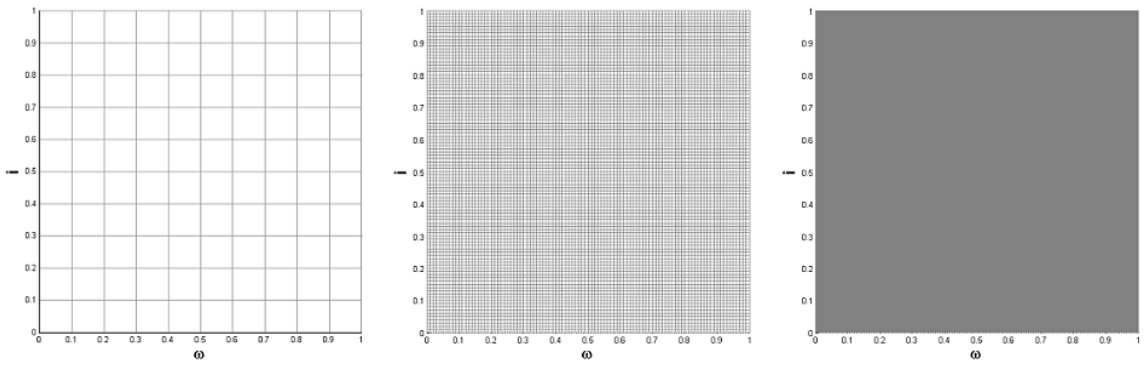

Figure 4.5. Grids used in the continuation map of periodic orbits.

The result is presented in figure 4.6.

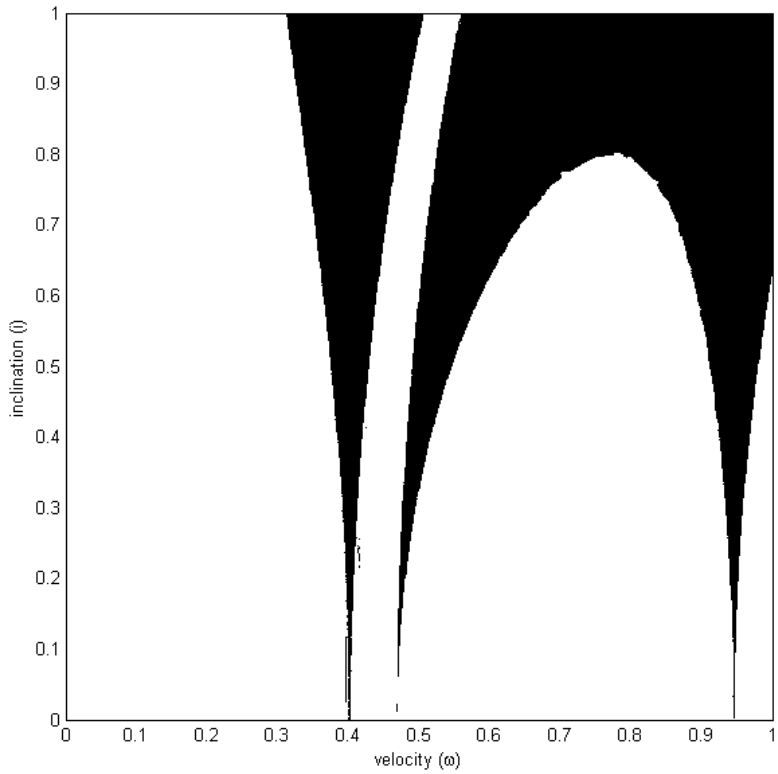

Figure 4.6. Continuation map of periodic orbits of critical point L_2. Black color represents the region where the method has not found the periodic orbit which replaces the L_2 point of RTBP.

Once we have all the periodic orbits in the parameter square $[0, 1] \times [0, 1]$ we can see how the orbits change in any way. For example, figure 4.7 corresponds to the orbits marked with asterisks on the map on figure 4.8. We can clearly see the gaps corresponding to the

tongues where there are not periodic orbits and how the shape of the orbits changes in the intermediate part.

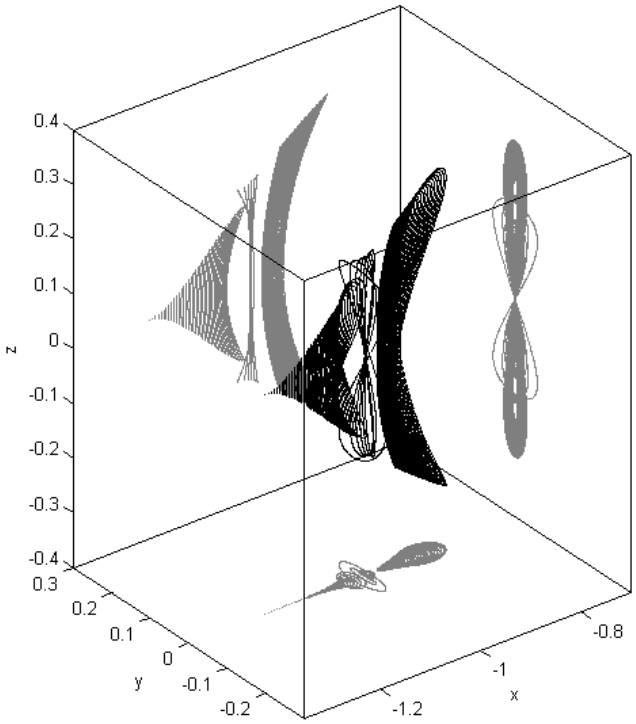

Figure 4.7. Path of periodic orbits marked with asterisks in figure 4.8 .

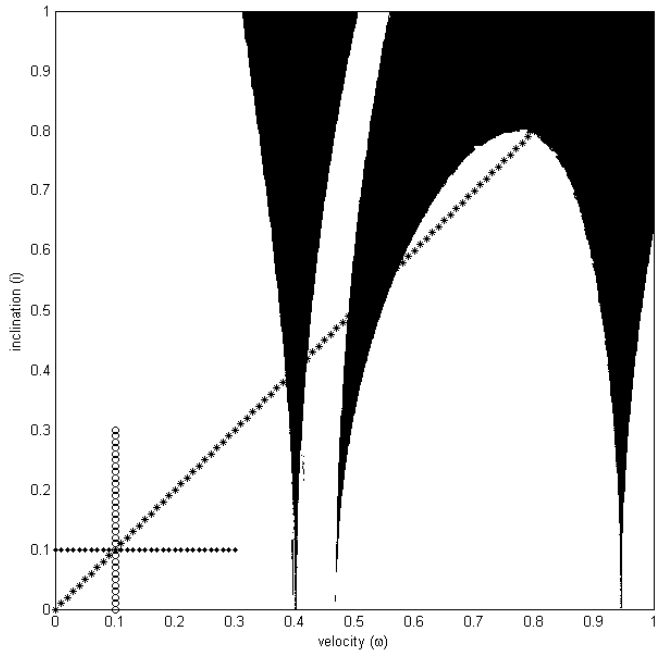

Figure 4.8. Continuation map highlighting the orbits represented in figures 4.3, 4.4 and 4.7.

4.2 The Rigid Body with Applied Torque RTBP

Model 2 was the first approach to model the precession phenomenon using the natural motion of a rigid body. Since we do not obtain the expected results after the first analysis of the problem, we decide to consider an external force to cause such motion of the primaries. Like the first model, we only have to take care of three parameters: the mean motion of the primaries, n, the maximum tilt angle achieved by a body with respect to the plane $z = 0$, α and a frequency of oscillation, β. In this model, the degenerate case when $\alpha = 0$, is equivalent to the RTBP with n as the mean motion of the primaries. The procedures used to compute the periodic orbits and the continuation are the same as those used in model 1.

4.2.1 Dynamical substitutes of critical points

Model 2 is very similar to model 1 in the sense that both models depends on two parameters. There is a parameter controlling the inclination (i in model 1 and α in model 2) and other which controls an angular velocity "of precession", ω in model 1, or a frequency of oscillation, β in model 2. In both cases the mean motion of the primaries, n, is set as 1 for simplicity. Another similarity is that both models consider an external force to cause the motion of the primaries which is not natural in the sense that there is a torque applied. Moreover, the equations of the models are not autonomous, so they are expected to have periodic orbits replacing the critical points existing in the case of no precession (RTBP).

Then, it is not a surprising fact that the periodic orbits obtained instead of L_2 point are very similar to those we got in model 1.

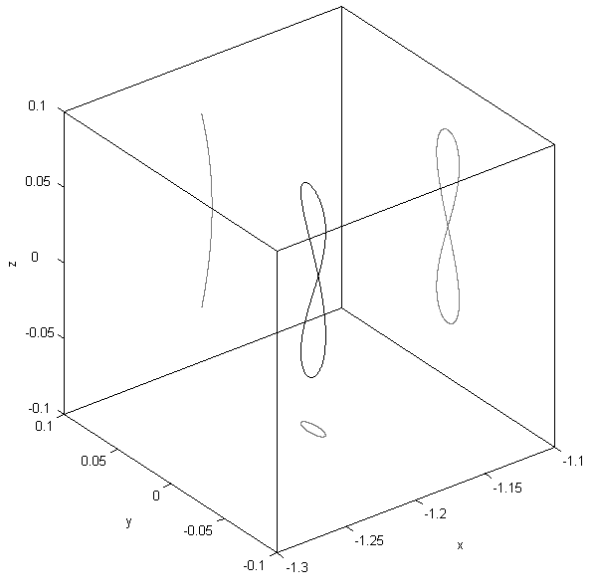

Figure 4.9. Periodic orbit substituting L_2 libration point and its projections obtained for the values $\alpha = 0.1$ and $\beta = 0.6$.

Notice that the orbit in figure 4.9 is not so slim as it was in model 1 but it is difficult to compare them taking into account that whereas the inclination is the same, the other parameter have a different meaning depending on the model. In this case, the orientation of the orbit is inverse with respect the orbit of model 1.

4.2.2 Continuation of orbits

In this model we can proceed as in the previous in order to see how the orbits depend on the parameters α and β. Let us fix one of the parameters while the other takes different values. Figures 4.10 and 4.11 consider both cases.

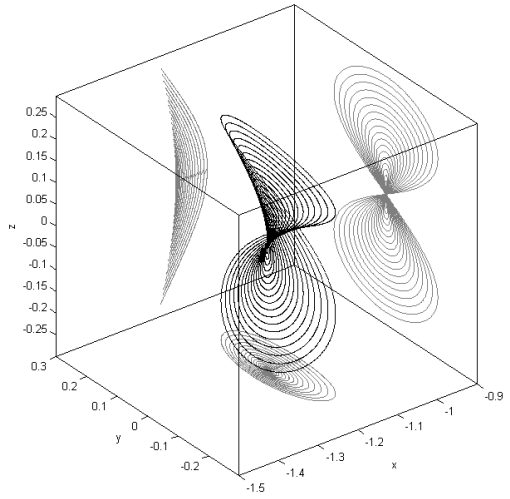

Figure 4.10. Family of periodic orbits with $\beta = 0.6$ and $\alpha \in [0, 0.4]$.

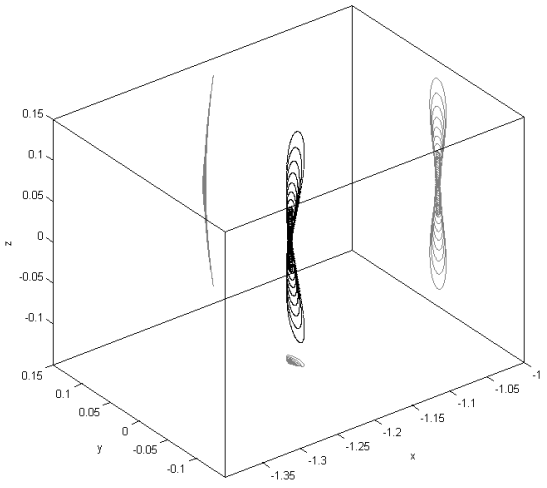

Figure 4.11. Family of periodic orbits with $\alpha = 0.1$ and $\beta \in [0.85, 1.15]$.

In figure 4.11 we can distinguish small orbits concentrated in the centre of the picture. They correspond to values of $\beta < 1$. As a consequence, their period is greater than the period of the revolving primary bodies which is 2π. However, they become considerably larger as the values of β are greater than the unit. In that case the period is smaller than 2π.

For the purpose of seeing the influence of the parameters we are going to compute the continuation map as we did with model 1. Notice that in this model we compute it in the square $[0.5, 1.25] \times [0, 0.4]$ because small values of β lead us to huge periods, since period is equal to $\frac{2\pi}{\beta}$, and because it is interesting to see the behaviour for values greater and lesser than 1. The inclination, α has to be small so a maximum of $\alpha = 0.4$, which means 22.92^{o}, is enough for our aspirations.

Again, some tongues appear in figure 4.12 and we suspect that the periodic orbits have different shapes depending on where the point (β, α) is located. Indeed, as shown in figure 4.13 the orientation of the periodic orbits change. It can be clearly seen in the projection on the corresponding y-plane.

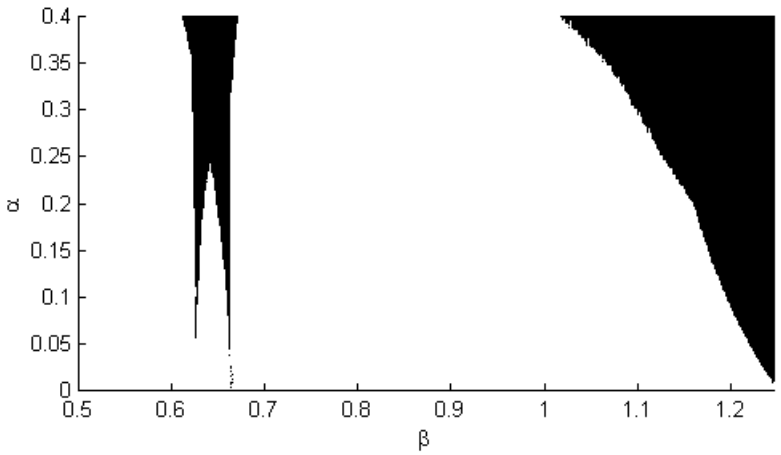

Figure 4.12. Continuation map of periodic orbits. Black color represents regions where the periodic orbits replacing L_2 do not exist.

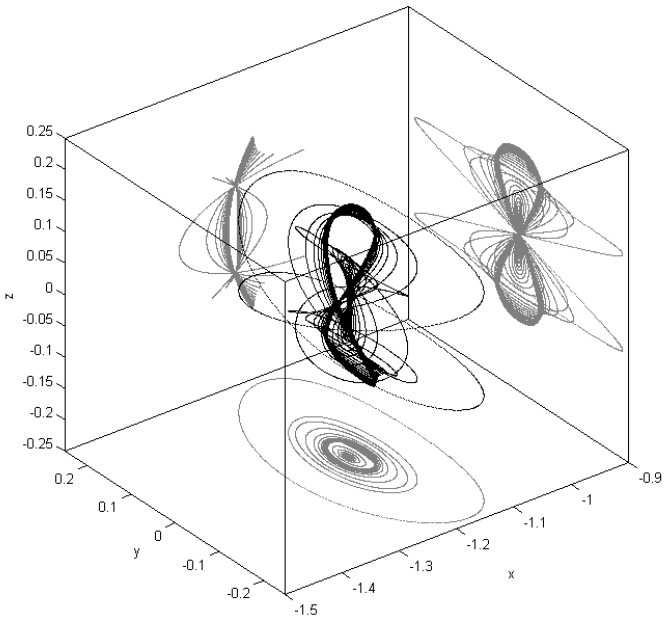

Figure 4.13. Path of periodic orbits marked with asterisks in figure 4.14.

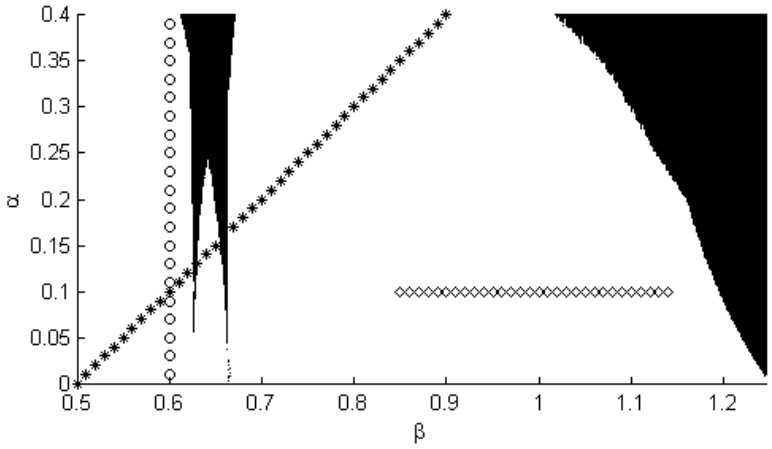

Figure 4.14. Continuation map highlighting the orbits represented in figures 4.10, 4.11 and 4.13.

4.3 The Rigid Body Torque-Free RTBP

The third model came from considering the same dynamics for a rigid body as in the second but thinking that although the motion of the primaries was not like we thought at first, it may cause the desired effect in the trajectories of the third body influenced by them. As we are going to see, indeed these trajectories will be different from what we

have seen in the results of the already mentioned papers of the introduction. Now we are restricted to the case of three bodies but afterwards we will develop this model in the context of galactic dynamics.

Unlike the previous models, now we have only two parameters: the mean motion of the primaries, n and the tilt angle of the bar which connects them, ε. Another difference is that the system of differential equations is autonomous. Therefore, it is interesting to compute the critical points. Then, using the Jacobi constant, we can obtain the zero-velocity curves. Finally, some studies are made around the periodic orbits we can find near the critical points. We study its dependence on ε and see how the stable and unstable manifold of a periodic orbit behave.

4.3.1 Critical Points

In the previous models we did not compute any critical point of their equations because they were expected to be (and they were actually) replaced by periodic orbits which we have computed in both cases. Now, due to the autonomy of the differential system these critical points may exist and the process of finding them is nearly the same as in the RTBP.

First of all, we set the vector field of the system equal to zero:

$$F(x_1, x_2, x_3, x_4, x_5, x_6) = \begin{pmatrix} F_1 \\ F_2 \\ F_3 \\ F_4 \\ F_5 \\ F_6 \end{pmatrix} = \mathbf{0}$$

where

$$\begin{aligned}
F_1 &= x_4, \\
F_2 &= x_5, \\
F_3 &= x_6, \\
F_4 &= 2\,n\,\cos(\varepsilon)\,x_5 + n^2\,\cos(\varepsilon)^2\,x_1 + n^2\,\sin(\varepsilon)\,\cos(\varepsilon)\,x_3 - n^2\left[(1-\mu)\frac{x_1-\mu}{r_1^3} + \mu\frac{x_1-\mu+1}{r_2^3}\right], \\
F_5 &= -2\,n\,\cos(\varepsilon)\,x_4 - 2\,n\,\sin(\varepsilon)\,x_6 + n^2\,x_2 - n^2\left[(1-\mu)\frac{x_2}{r_1^3} + \mu\frac{x_2}{r_2^3}\right], \\
F_6 &= 2\,n\,\sin(\varepsilon)\,x_5 + n^2\,\sin(\varepsilon)\,\cos(\varepsilon)\,x_1 + n^2\,\sin(\varepsilon)^2\,x_3 - n^2\left[(1-\mu)\frac{x_3}{r_1^3} + \mu\frac{x_3}{r_2^3}\right].
\end{aligned}$$

In this way, we find that the velocity part is null ($x_4 = x_5 = x_6 = 0$) and the significant equations rest as follows:

$$n^2\,\cos(\varepsilon)^2\,x_1 + n^2\,\sin(\varepsilon)\,\cos(\varepsilon)\,x_3 - n^2\left[(1-\mu)\frac{x_1-\mu}{r_1^3} + \mu\frac{x_1-\mu+1}{r_2^3}\right] = 0, \qquad (4.1)$$

$$n^2\, x_2 - n^2 \left[(1-\mu)\frac{x_2}{r_1^3} + \mu\frac{x_2}{r_2^3} \right] = 0, \tag{4.2}$$

$$n^2\, \sin(\varepsilon)\, \cos(\varepsilon)\, x_1 + n^2\, \sin(\varepsilon)^2\, x_3 - n^2 \left[(1-\mu)\frac{x_3}{r_1^3} + \mu\frac{x_3}{r_2^3} \right] = 0. \tag{4.3}$$

Now, the analysis forks in two ways. Imagine that in the first place $x_2 \neq 0$. From equation (4.2):

$$1 - \frac{1-\mu}{r_1^3} - \frac{\mu}{r_2^3} = 0. \tag{4.4}$$

From (4.1), (4.3) and (4.4) we finally get

$$\begin{aligned} x_1 &= \mu - \frac{1}{2}, \\ x_2 &= \pm\sqrt{\frac{3}{4} - \tan^2(\varepsilon)\left(\mu - \frac{1}{2}\right)^2}, \\ x_3 &= \tan(\varepsilon)\left(\mu - \frac{1}{2}\right). \end{aligned}$$

In case that $\varepsilon = 0$, these coordinates correspond to equilateral points of the RTBP.

If $x_2 = 0$, then equations (4.1) and (4.3) lead us to a non-linear system and it is necessary a numerical method to find the coordinates of the critical points. When $\varepsilon = 0$, $x_3 = 0$ and this system becomes the Euler quintic whose solutions are the coordinates x_1 of the collinear points in the RTBP. We take these solutions as the initial condition for the Newton method that we use to find the coordinates of the collinear critical points of the model 3.

Therefore, we have five critical points and their coordinates slightly vary from those of the RTBP. We can see its disposition in figure 4.15.

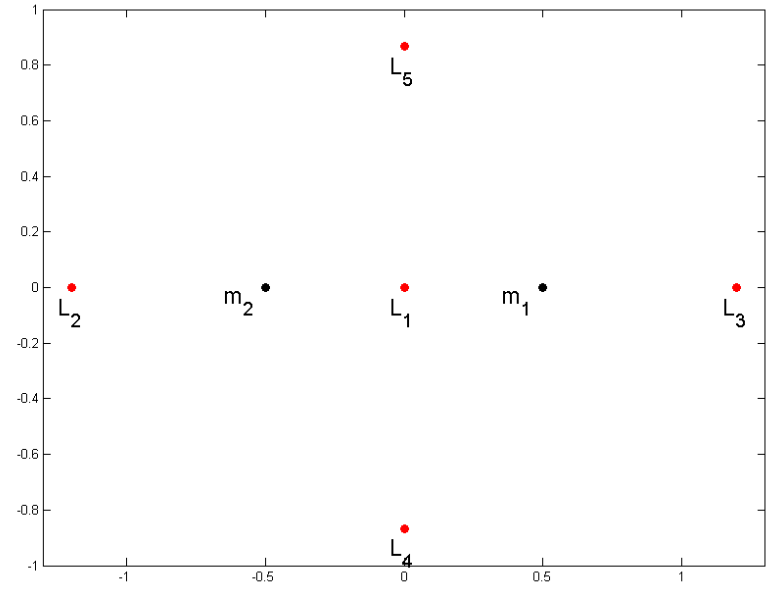

Figure 4.15. Critical points of model 3 with respect to the primaries (case $\mu = \frac{1}{2}$) in body coordinates.

For example, in figure 4.16 we can see how the coordinates of a critical point vary as the value of ε change.

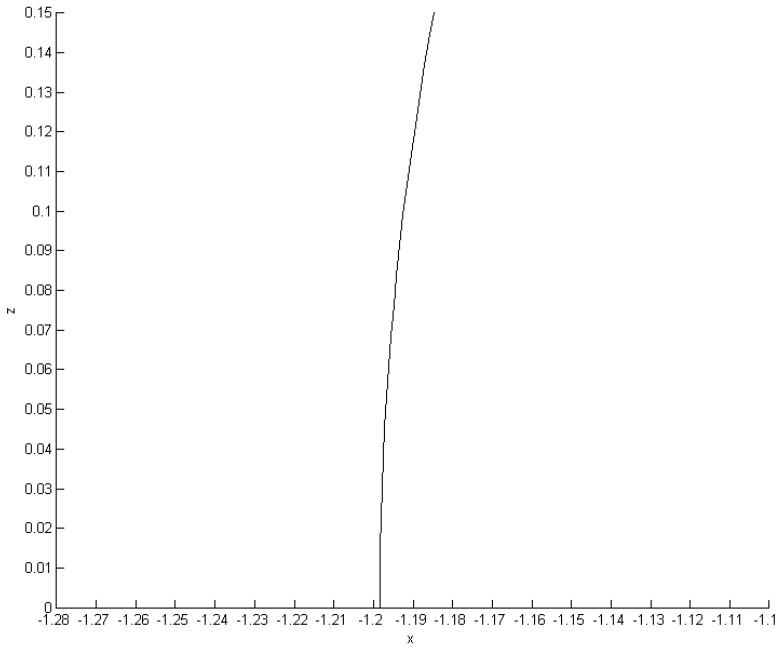

Figure 4.16. Coordinates of L_2 as the value of ε change from 0 to -0.2.

4.3.2 Zero-velocity curves

In this model, the Jacobi constant does not have an explicit dependence on time. Therefore, given a fixed level of energy, i.e., a fixed value of the Jacobi constant, we could

compute the zero-velocity surface. This surface is obtained by assuming that the velocity variables are null and it divides the space into two regions: the permitted and the forbidden. The zero-velocity curves are contour lines of this surface. In a certain plane, they delimit the regions where the third body is allowed to move and the regions where not. For example, in the RTBP, taking $\mu < \frac{1}{2}$, the zero-velocity curves in the plane $z = 0$ are shown in figure 4.17.

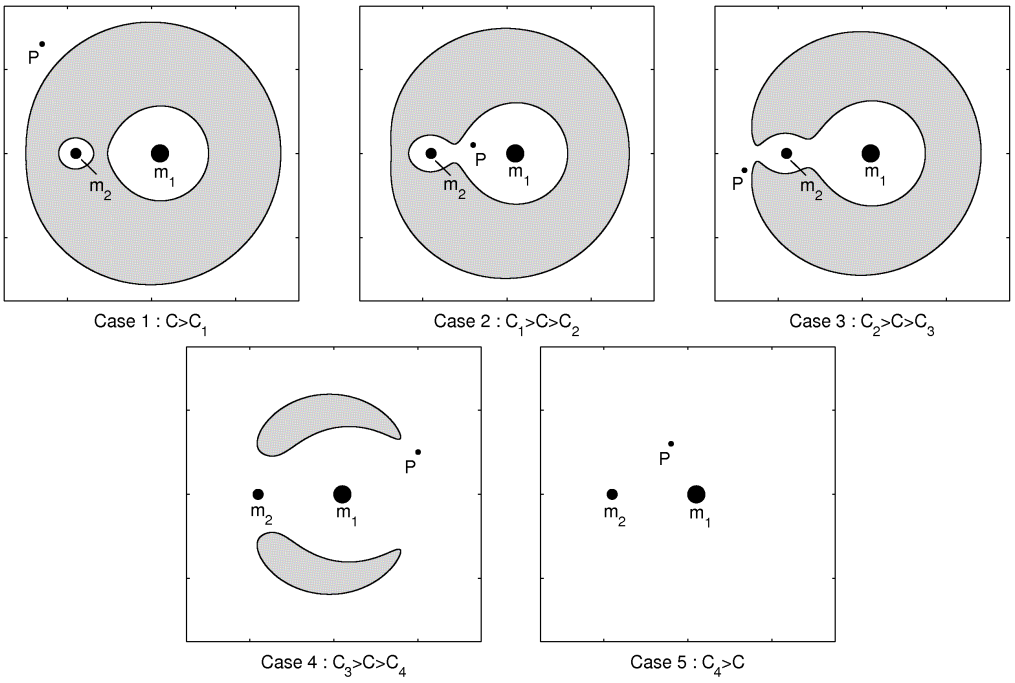

Figure 4.17. Zero-velocity curves for the RTBP ($z = 0$). Grey regions are forbidden to the third body.

Each case depends on the value we give to C (or more precisely, the energy of the third body) and C_1, C_2, C_3, C_4, C_5 are the values of the Jacobi constant in the critical points.

The method of computing the zero-velocity curve is as simple as finding the roots of the Jacobi constant once we have taken null the velocities. Thus, we will use a Newton method being aware that sometimes it could be tricky to deal with the critical points of the curve.

In model 3 we obtain nearly the same plot as in the RTBP, taking into account that we are interested in a symmetric distribution of the primaries, i.e., $\mu = \frac{1}{2}$. It seems that the parameter ε would have to affect in some way the zero-velocity curve because in model 3 the primaries are tilted with respect the plane $z = 0$. In the RTBP($\mu = \frac{1}{2}$), if we take other plane as a reference, the curves are symmetric with $y = 0$ as its axis of symmetry. In model 3 this symmetry is broken due to the inclination of the bodies, as we can observe in figures 4.19 and 4.20. However, figure 4.18 shows a symmetric zero-velocity curve.

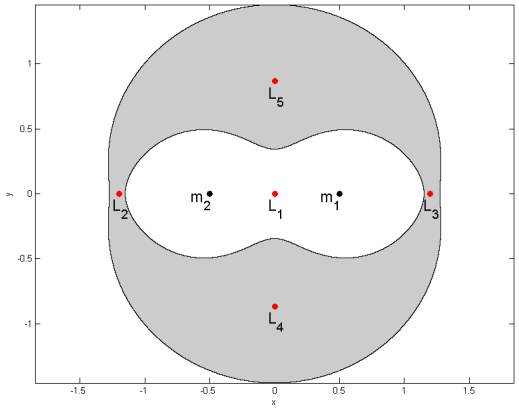

Figure 4.18. Zero-velocity curve of model 3 (case 4) with $z = 0$.

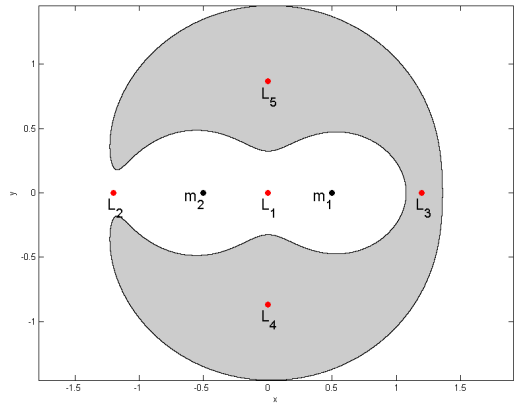

Figure 4.19. Zero-velocity curve of model 3 (case 4) with $z = 0.1$.

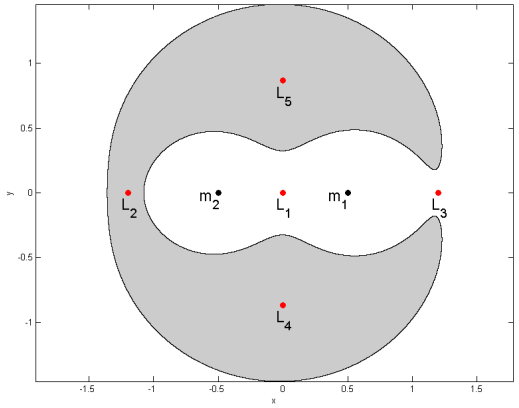

Figure 4.20. Zero-velocity curve of model 3 (case 4) with $z = -0.1$.

4.3.3 Lyapunov orbits

Model 3 does not have the orbits which substitute the critical points like in the other models. However, we can compute the Lyapunov orbits with the objective of seeing how they behave under the precession phenomenon. There are two types of Lyapunov orbits: the vertical and the horizontal. In the RTBP horizontal Lyapunov orbits reside in the plane $z = 0$ and orthogonally traverse the x axis. It is natural that a perturbation of these orbits also exists in model 3.

The first thing to do is to calculate a linear approximation of the vector field of the model. Therefore we need to linearize the model taking its differential in the critical point where we want to find the Lyapunov orbit. It is convenient to do this analysis around L_2 or L_3 because these points are at the end of the body (the two spheres connected by a massless bar) and this will connect with the galactic dynamics later.

$$\dot{X} = DF(X_{L_i})\, X \tag{4.5}$$

In equation (4.5), X means $(x_1, x_2, x_3, x_4, x_5, x_6)^T$ and X_{L_i} are the coordinates of the critical point L_2 or L_3. We are going to consider only L_2 because the case L_3 is analogous. Then, the differential of the vector field in L_2 is

$$DF(X_{L_2}) = \begin{pmatrix} 0 & 0 & 0 & 1 & 0 & 0 \\ 0 & 0 & 0 & 0 & 1 & 0 \\ 0 & 0 & 0 & 0 & 0 & 1 \\ a & 0 & d & 0 & e & 0 \\ 0 & b & 0 & -e & 0 & -f \\ d & 0 & c & 0 & f & 0 \end{pmatrix},$$

where

$$\begin{aligned} a &= n^2 \cos^2(\varepsilon) + \left.\frac{\partial^2 U}{\partial x_1^2}\right|_{L_2}, \\ b &= n^2 + \left.\frac{\partial^2 U}{\partial x_2^2}\right|_{L_2}, \\ c &= n^2 \sin^2(\varepsilon) + \left.\frac{\partial^2 U}{\partial x_3^2}\right|_{L_2}, \\ d &= n^2 \sin(\varepsilon)\cos(\varepsilon) + \left.\frac{\partial^2 U}{\partial x_1 x_3}\right|_{L_2}, \\ e &= 2\,n\cos(\varepsilon), \\ f &= 2\,n\sin(\varepsilon). \end{aligned}$$

Using a computer algebra system like Maple is very useful to determine the linear solution of the system (4.5). Once we know the shape of the matrix $DF(X_{L_2})$ and the values that take a, b, c, d, e and f, it is quite easy to find its eigenvalues: λ_0, $-\lambda_0$, $\omega_0\, i$, $-\omega_0\, i$, $\nu_0\, i$ and $-\nu_0\, i$ with $\lambda_0, \omega_0, \nu_0 \in \mathbb{R}$. So a common way of writing the solution according to the

RTBP[8] is

$$\begin{aligned}
x_1(t) &= \alpha_1\,\mathbf{e}^{\lambda_0\,t} + \alpha_2\,\mathbf{e}^{-\lambda_0\,t} + \alpha_3\,\cos(\omega_0\,t+\phi_1) + k_3\,\alpha_4\,\cos(\nu_0\,t+\phi_2),\\
x_2(t) &= \bar{k_2}\,\alpha_1\,\mathbf{e}^{\lambda_0\,t} - \bar{k_2}\,\alpha_2\,\mathbf{e}^{-\lambda_0\,t} + \bar{k_1}\,\alpha_3\,\sin(\omega_0\,t+\phi_1) + \bar{k_3}\,\alpha_4\,\sin(\nu_0\,t+\phi_2),\\
x_3(t) &= \bar{\bar{k_2}}\,\alpha_1\,\mathbf{e}^{\lambda_0\,t} - \bar{\bar{k_2}}\,\alpha_2\,\mathbf{e}^{-\lambda_0\,t} + \bar{\bar{k_1}}\,\alpha_3\,\cos(\omega_0\,t+\phi_1) + \alpha_4\,\cos(\nu_0\,t+\phi_2),\\
x_4(t) &= \dot{x}_1,\\
x_5(t) &= \dot{x}_2,\\
x_6(t) &= \dot{x}_3.
\end{aligned}$$

Phases in the trigonometric expressions can be avoided by writing the solution in the following way:

$$\begin{aligned}
x_1(t) &= \beta_1\,\mathbf{e}^{\lambda_0\,t} + \beta_2\,\mathbf{e}^{-\lambda_0\,t} + \beta_3\,\cos(\omega_0\,t) + \beta_4\,\sin(\omega_0\,t) + p_3\,\beta_5\,\cos(\nu_0\,t) + p_3\,\beta_6\,\sin(\nu_0\,t),\\
x_2(t) &= \bar{p_2}\,\beta_1\,\mathbf{e}^{\lambda_0\,t} - \bar{p_2}\,\beta_2\,\mathbf{e}^{-\lambda_0\,t} + \bar{p_1}\,\beta_3\,\sin(\omega_0\,t) - \bar{p_1}\,\beta_4\,\cos(\omega_0\,t) + \bar{p_3}\,\beta_5\,\sin(\nu_0\,t)\\
&\quad -\bar{p_3}\,\beta_6\,\cos(\nu_0\,t),\\
x_3(t) &= \bar{\bar{p_2}}\,\beta_1\,\mathbf{e}^{\lambda_0\,t} + \bar{\bar{p_2}}\,\beta_2\,\mathbf{e}^{-\lambda_0\,t} + \bar{\bar{p_1}}\,\beta_3\,\cos(\omega_0\,t) + \bar{\bar{p_1}}\,\beta_4\,\sin(\omega_0\,t) + \beta_5\,\cos(\nu_0\,t)\\
&\quad +\beta_6\,\sin(\nu_0\,t),\\
x_4(t) &= \dot{x}_1,\\
x_5(t) &= \dot{x}_2,\\
x_6(t) &= \dot{x}_3.
\end{aligned}$$

Remark. Notice that the expressions $A\cos(\omega\,t+\phi)$ and $B\cos(\omega\,t)+C\sin(\omega\,t)$ are equivalent with the change $\phi = \arctan\left(\frac{-C}{B}\right)$ and $A = \sqrt{B^2+C^2}$. Something similar happens with $A\sin(\omega\,t+\phi)$.

k_3, $\bar{k_1}$, $\bar{k_2}$, $\bar{k_3}$, $\bar{\bar{k_1}}$, $\bar{\bar{k_2}}$, p_3, $\bar{p_1}$, $\bar{p_2}$, $\bar{p_3}$, $\bar{\bar{p_1}}$ and $\bar{\bar{p_2}}$ are constants depending on a, b, c, d, e and f. Moreover, α_i, β_i and ϕ_i are arbitrary values.

If we want to compute horizontal Lyapunov orbits of our model 3, we have to begin with their linear approximation and then refine it to obtain the orbit of the non-linear system. The linear solution have three different parts. The exponential part is related to the stable and unstable manifolds and we will ignore this part. This is reached by assuming that $\beta_1 = \beta_2 = 0$. The other two parts are related to the frequencies. We are going to work only with one frequency so taking $\beta_5 = \beta_6 = 0$ the solution remains as

$$\begin{aligned}
x_1(t) &= \beta_3\,\cos(\omega_0\,t) + \beta_4\,\sin(\omega_0\,t),\\
x_2(t) &= \bar{p_1}\,\beta_3\,\sin(\omega_0\,t) - \bar{p_1}\,\beta_4\,\cos(\omega_0\,t),\\
x_3(t) &= \bar{\bar{p_1}}\,\beta_3\,\cos(\omega_0\,t) + \bar{\bar{p_1}}\,\beta_4\,\sin(\omega_0\,t),\\
x_4(t) &= \dot{x}_1,\\
x_5(t) &= \dot{x}_2,\\
x_6(t) &= \dot{x}_3.
\end{aligned}$$

Now, taking into account that at $t = 0$ the solution must have only x and z components and leave with velocity only in the y component (transversal to the x axis), we realize that

[8]The expression of the solution corresponding to the RTBP can be found in [14].

we have to take $\beta_4 = 0$ and give an arbitrary value to β_3. Moreover the resultant orbit is centred in the origin and it must be actually around the critical L_2 point. Therefore we only have to add to the solution the components of $L_2 = (x_1^{L_2}, 0, x_3^{L_2}, 0, 0, 0)$.

$$\begin{aligned} x_1(t) &= x_1^{L_2} + \beta_3 \cos(\omega_0 t), \\ x_2(t) &= \bar{p_1}\, \beta_3 \sin(\omega_0 t), \\ x_3(t) &= x_3^{L_2} + \bar{\bar{p_1}}\, \beta_3 \cos(\omega_0 t), \\ x_4(t) &= \dot{x}_1, \\ x_5(t) &= \dot{x}_2, \\ x_6(t) &= \dot{x}_3. \end{aligned}$$

Figure 4.21 shows a linear orbit taking $\beta_3 = 10^{-2}$. It can be suspected from the $x - z$ and $y - z$ projection that the orbit is contained in a plane which is not perpendicular to $z = 0$ but it seems to be tilted.

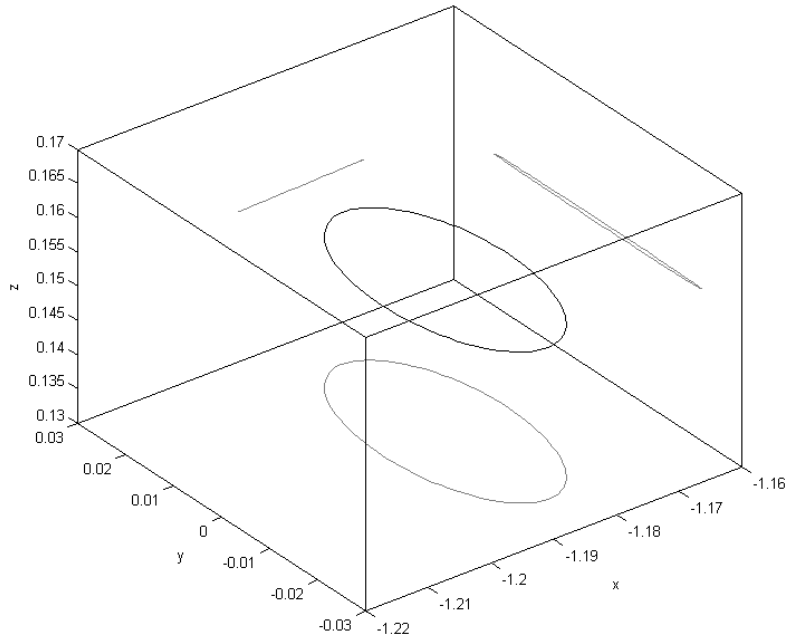

Figure 4.21. Approximation to a Lyapunov orbit and its projections with $\varepsilon = -0.2$.

Once we have the linear approximation, we refine it to obtain the horizontal Lyapunov orbit of the non-linear system. The procedure of refinement is a parallel shooting method as the explained previously but introducing an important change. We add an equation to the system in order to preserve the energy of the orbit, this is, the refined orbit and the linear approximation have the same energy. In this case, the initial conditions are the points of the linear orbit and the result the non-linear orbit with the same Jacobi constant (figure 4.22).

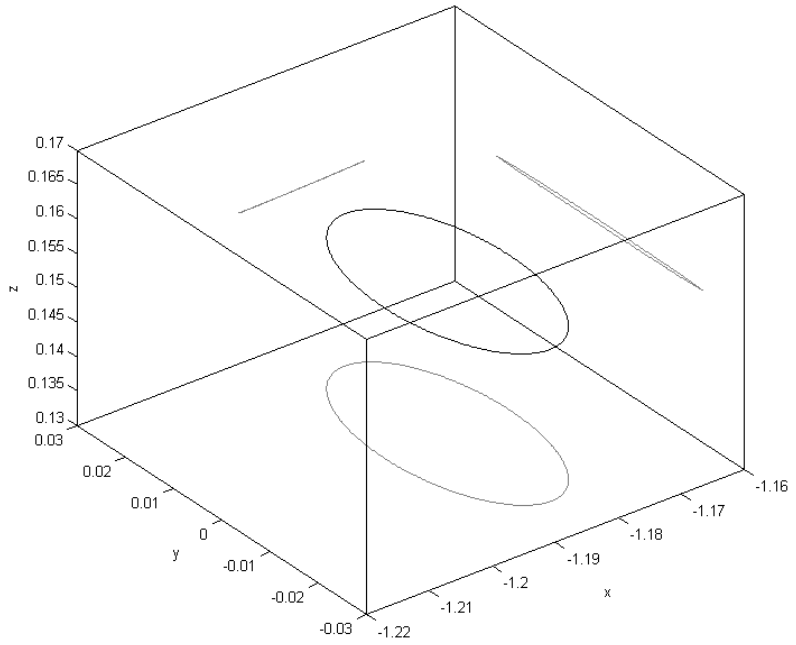

Figure 4.22. Lyapunov orbit and its projections with $\varepsilon = -0.2$.

It is difficult to see any difference with respect to the orbit shown in figure 4.21 which means that the orbit from the linear systems is a good approximation. However, as we will see later, these non-linear orbits cannot be embedded in a plane.

4.3.4 Continuation of Lyapunov orbits

Here, the objective is to find a family of Lyapunov orbits varying the parameter ε from -0.2 to 0. Again, we use the parallel shooting method fixing the energy. For a given value of ε, ε_i, we take as initial condition the orbit computed for ε_{i-1} and refine it using the parallel shooting method. Then, this orbit will be used as initial condition for ε_{i+1}. All the obtained orbits have the same energy since the method obliges it now.

Figure 4.23 shows the family of horizontal Lyapunov orbits obtained from this method.

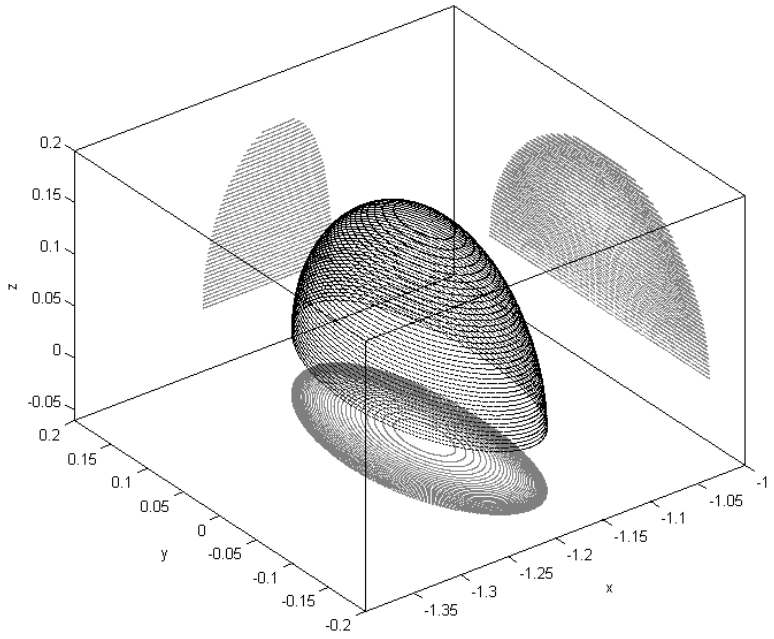

Figure 4.23. Family of horizontal Lyapunov orbits and its projections with $\varepsilon \in [-0.2, 0]$.

4.3.5 Stable and unstable manifolds

In previous sections we have computed some periodic orbits near the critical points of model 3. Like the critical points, these orbits have a related stable and unstable manifolds. The aim of this section is to compute these manifolds and see how they behave depending on the parameter ε. We can achieve this objective by means of the following procedure.

First of all let us take a fix value of ε. For instance, we are going to do all the calculations for $\varepsilon = -0.2$ (an inclination of 11.46°). Then, we take the periodic orbit previously computed (from now, called γ_ε) for this value and its monodromy matrix. If we call p the period of the orbit, this matrix is the solution at $t = p$ of the differential system corresponding to the variational equations of model 3 system. In other words, if we take the differential of the vector field from the equations of model 3, then its solution (which is a matrix) at time the period of the orbit is the monodromy matrix. Once we have the monodromy matrix, $\mathbf{M}(p)$, we compute its eigenvalues and eigenvectors. We are interested in the asymptotic part represented by two real eigenvalues. The unstable manifold will come from the real eigenvalue which is in norm bigger than the unit. The other real eigenvalue is related to the stable manifold. Let us assume that these eigenvalues are respectively ρ_1 and ρ_2 with associated eigenvectors $\mathbf{v_1}$ and $\mathbf{v_2}$.

The second part of the procedure consists in computing k trajectories which will represent the manifolds. We are going to explain it for the unstable case, taking into account that the stable case is analogous. Consider $t_i = \frac{ip}{k}$ with $i = 0, \ldots, k$. In this way, t_k is the period. If the orbit γ_ε is parametrised by $\mathbf{x}(t)$, then $\mathbf{x}(t_i)$ are k different points over γ_ε since $\mathbf{x}(t_0) = \mathbf{x}(t_k)$ (γ is a periodic orbit). Now, consider $\mathbf{v^u}(t)$ the vector corresponding to the unstable eigenvalue ρ_1 transported by means of $\mathbf{M}(t)$, i.e.,

$\mathbf{v^u}(t) = \mathbf{M}(t)\mathbf{v_1}$. $\mathbf{M}(t)$ was the solution of the variational equations which have initial condition $\mathbf{M}(0) = \mathbf{Id}$, the identity matrix. Therefore, $\mathbf{v^u}(0) = \mathbf{v_1}$. These k different vectors will allow us to have k different points to integrate in the equations of the model:

$$\mathbf{x_i} = \mathbf{x}(t_i) + \delta \mathbf{v^u}(t_i).$$

δ is a real value and must be small (10^{-2}, 10^{-3}, ...). The resultant trajectories are the unstable manifold (figures 4.24 and 4.25).

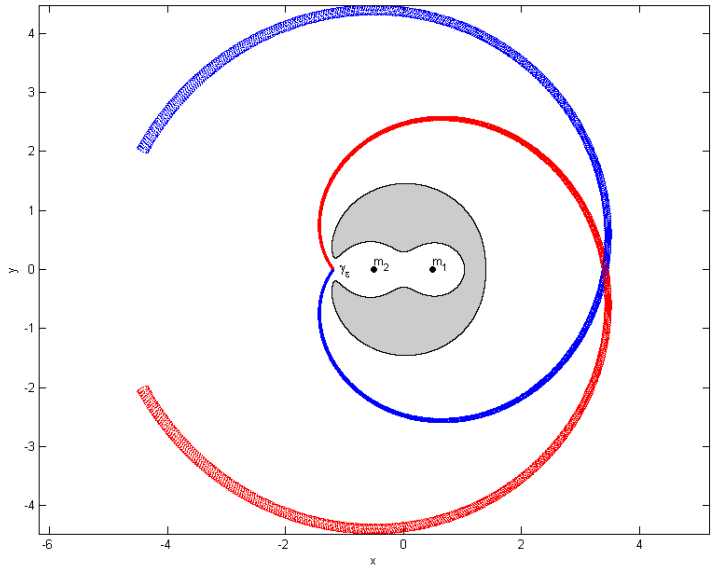

Figure 4.24. Stable (blue) and unstable (red) manifolds of the orbit γ_ε with $\varepsilon = -0.2$.

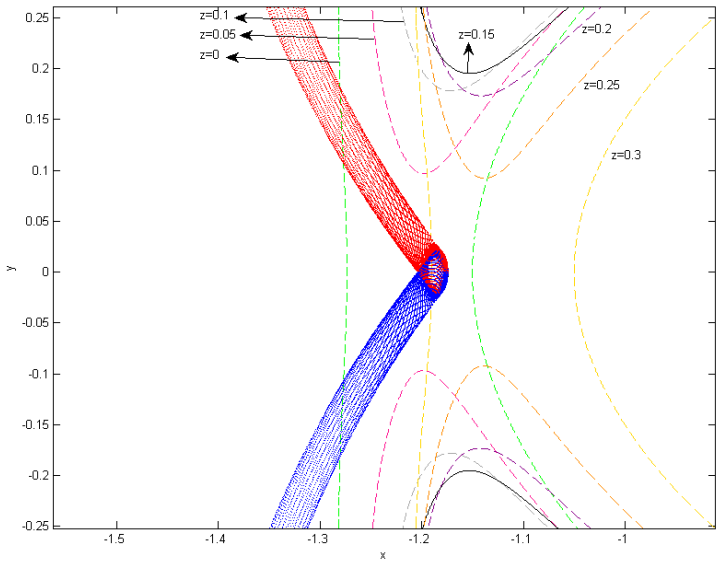

Figure 4.25. Stable (blue) and unstable (red) manifolds of the orbit γ_ε and some zero-velocity curves corresponding to different values of z.

In the previous figures we have only represented the exterior branches of the stable and unstable manifolds. Although we are more interested them, we present the inner branches in figure 4.26.

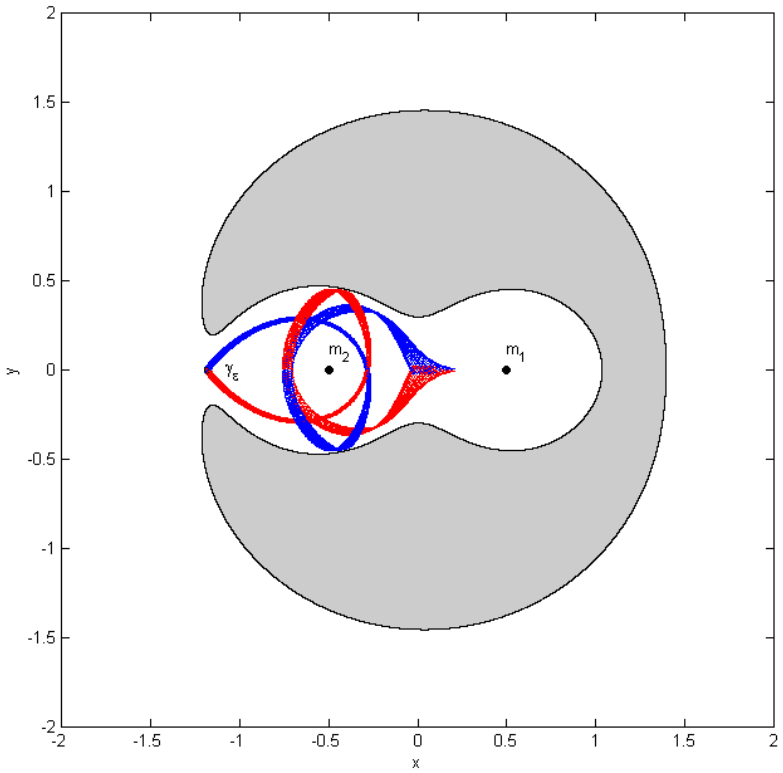

Figure 4.26. Inner branches of the stable (blue) and unstable (red) manifolds of the orbit γ_ε with $\varepsilon = -0.2$.

4.4 The Precessing Miyamoto-Nagai Ferrers model

The galactic model is an adaptation of model 3 to the galactic context. Therefore, the results are similar to those presented in model 3. However, it is important to notice the differences caused by the change of the potential; the disc and the bar added to the precession inflict a significant behaviour in the asymptotic manifolds of Lyapunov orbits. Another thing to bear in mind is the influence of the parameters. Apart from the parameter ε, the parameters related to the shape of the bar and the disc and the masses of both have an influence on the shape of the manifolds. We invite the reader to consult [15] in order to obtain further information on the parameters of the potentials Ferrers and Miyamoto-Nagai and on the dynamics in a barred galaxy, related to the manifolds corresponding to the orbits near the critical points. Moreover, the parameters and the table below are extracted from there.

In this section we are going to compute the critical points of the galactic model, the zero-velocity surfaces, the Lyapunov orbits and their dependence on the parameter ε and the stable and unstable manifolds of these orbits. There are some typical values of the parameters a_b, b_b, c_b, a_d, b_d, m_b, m_d and n corresponding to different shapes of

barred galaxies. The first five are taken as $a_b = 6$, $b_b = 1.5$, $c_b = 0.6$, $a_d = 3$, $b_d = 1$, in all the cases and the rest from the following table:

Galaxy type	m_b	m_d	n
R_1 ring	0.1	0.9	0.05471
R_2 ring	0.4	0.6	0.06
R_1 pseudo-ring	0.3	0.7	0.051
Closed spiral	0.3	0.7	0.06
Open spiral	0.4	0.6	0.055

For the following calculations we are going to take the values corresponding to an open spiral galaxy.

4.4.1 Critical points

Critical points of model 3 and galactic model have the same disposition. However, in the second case they are consistent with the longitude of the bar. Figures 4.27 and 4.28 represent different views of this disposition. Notice, from figure 4.28, that whereas L_1, L_4 and L_5 maintain their coordinates fixed, L_2 and L_3 vary as ε decrease.

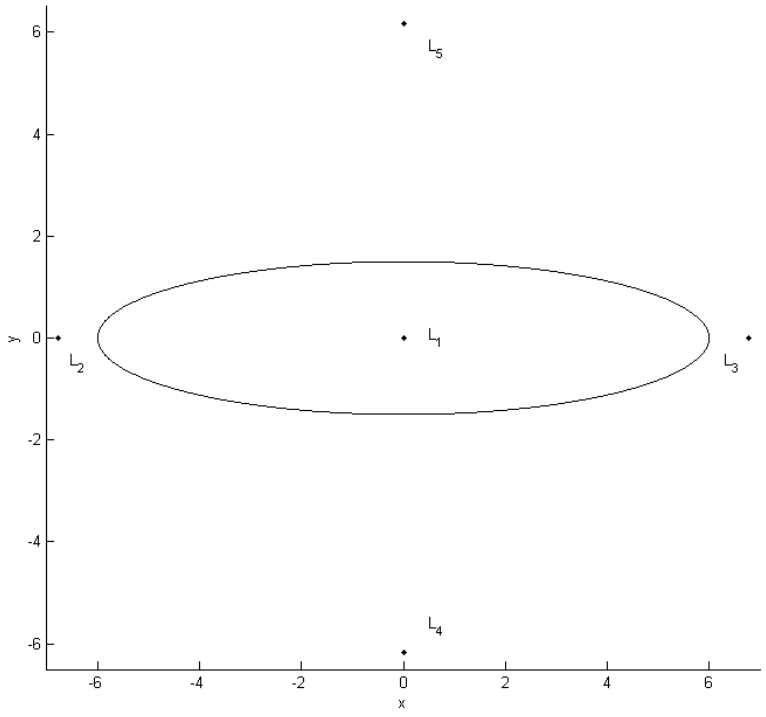

Figure 4.27. $x - y$ view of critical points from galactic model with $\varepsilon \in [-0.2, 0]$.

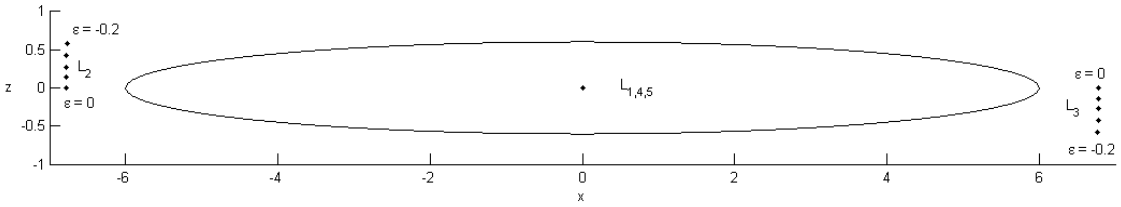

Figure 4.28. $x - z$ view of critical points from galactic model with $\varepsilon \in [-0.2, 0]$.

4.4.2 Zero-velocity surfaces

The zero-velocity surfaces in this model suppose a constraint in the motion of a particle submitted to the influence of the galaxy. Like the zero-velocity curves, there are different cases depending on the value of the energy and their topology can be inferred from the planar cases. For example, in figure 4.29 we have the zero-velocity surface corresponding to the case 4. It can clearly be seen in figure 4.30 the similarity with the zero-velocity curves we had in model 3. Notice the holes connecting the exterior and inner region.

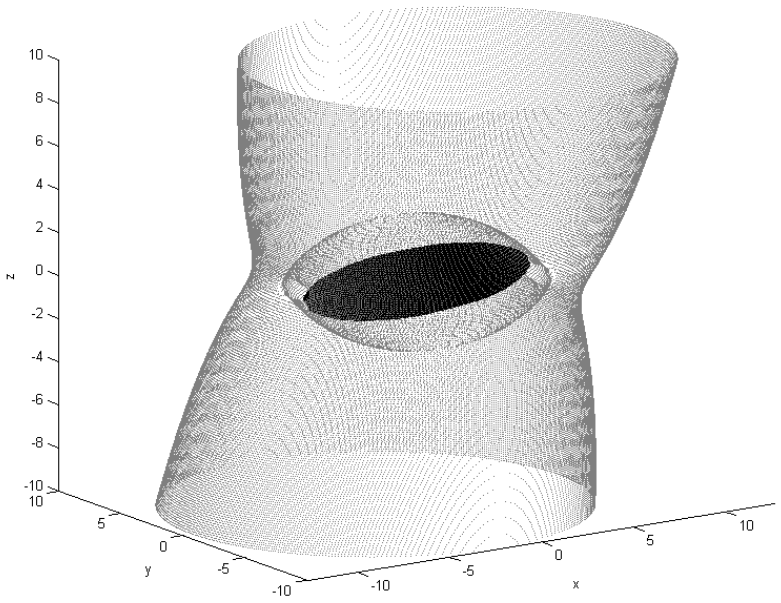

Figure 4.29. 3D view of the bar and the zero-velocity surface corresponding to a value of the Jacobi constant of $C = -0.20901$ and $\varepsilon = -0.2$.

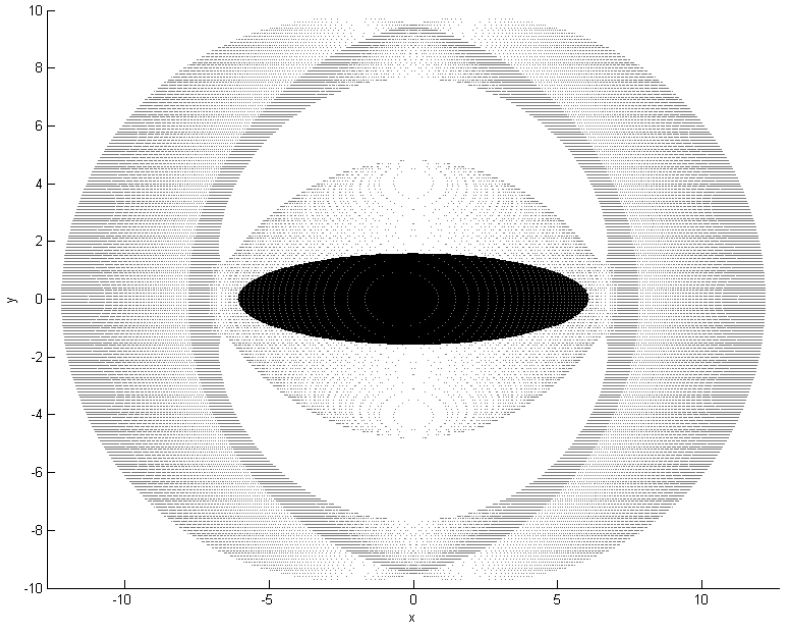

Figure 4.30. $x - y$ view of the zero-velocity surface.

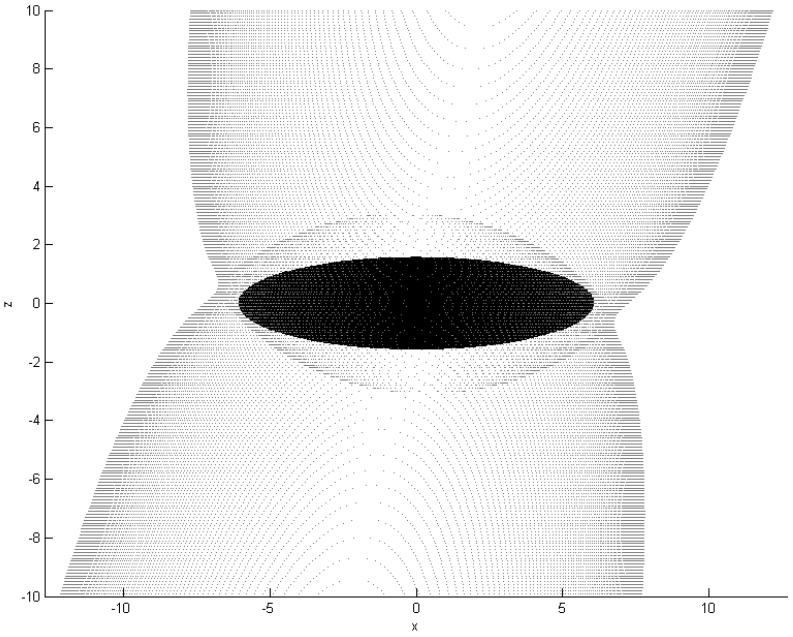

Figure 4.31. $x - z$ view of the zero-velocity surface.

4.4.3 Lyapunov orbits

The Lyapunov orbits of this model can be computed using all the resources we had in model 3. These orbits are located near the critical points L_2 and L_3, in the entrances of the inner region. Now we can see the importance that these orbits, or more concretely, their stable and unstable manifolds, may have in the flow of stars from the nucleus to

the arms and viceversa. In figure 4.32 we can observe again that the orbit is not planar. Figure 4.33 shows the location of these orbits with respect the zero-velocity surface.

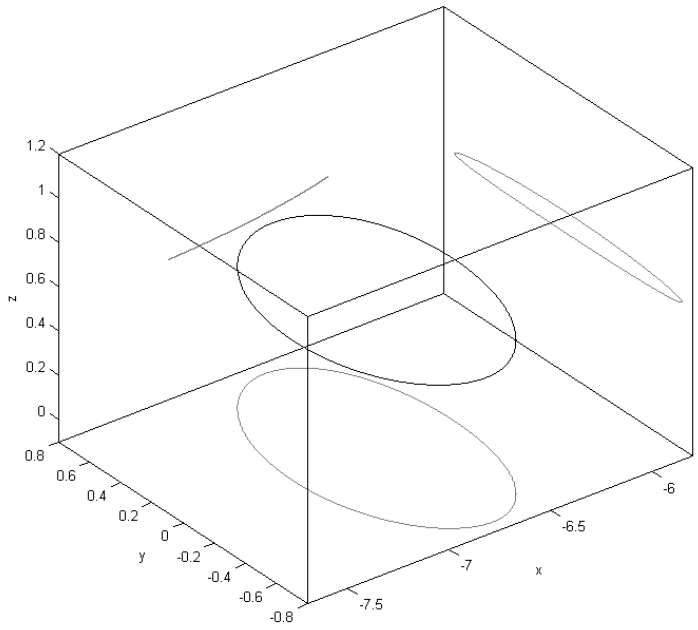

Figure 4.32. Horizontal Lyapunov periodic orbit near L_2 and its projections with $\varepsilon = -0.2$.

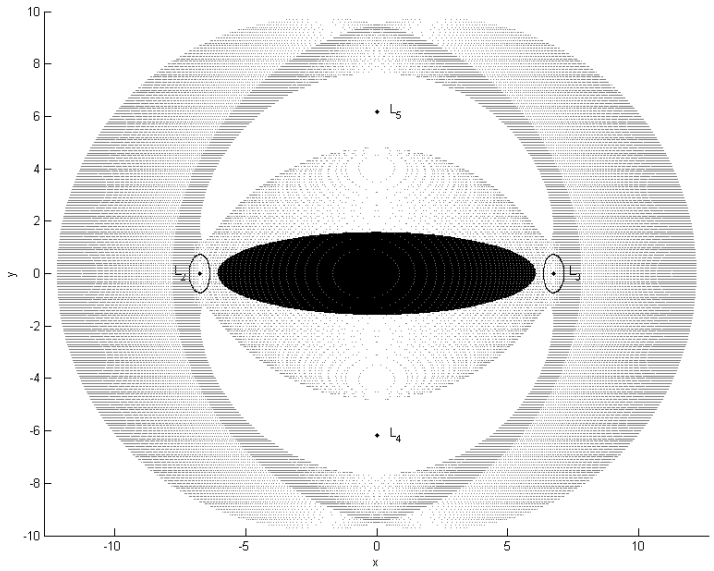

Figure 4.33. Location of Lyapunov orbits of L_2 and L_3 points with respect the zero-velocity surface.

Now, we present a table expressing some the values of the constants from the linear solution as well as the values of the eigenvalues for each value of ε.

Table 4.1: Values of the eigenvalues and the constants from the expression of the linear solution.

ε	λ	ω	ν	p_3	$\bar{p_1}$	$\bar{p_2}$	$\bar{p_3}$	$\bar{\bar{p}}_1$	$\bar{\bar{p}}_2$
0.000000	0.041852	0.069207	0.087428	0.000000	-1.930751	-1.771831	0.000000	0.000000	0.000000
-0.010000	0.041846	0.069202	0.087401	-0.000645	-1.930608	-1.772148	0.015066	0.004715	-0.005534
-0.020000	0.041826	0.069187	0.087320	-0.001304	-1.930177	-1.773098	0.030182	0.009456	-0.011085
-0.030000	0.041792	0.069163	0.087185	-0.001990	-1.929454	-1.774685	0.045395	0.014249	-0.016669
-0.040000	0.041746	0.069129	0.086997	-0.002720	-1.928435	-1.776912	0.060757	0.019120	-0.022304
-0.050000	0.041686	0.069086	0.086757	-0.003508	-1.927112	-1.779786	0.076319	0.024098	-0.028007
-0.060000	0.041612	0.069033	0.086466	-0.004371	-1.925473	-1.783315	0.092135	0.029211	-0.033794
-0.070000	0.041526	0.068970	0.086124	-0.005328	-1.923506	-1.787507	0.108262	0.034491	-0.039684
-0.080000	0.041427	0.068899	0.085734	-0.006399	-1.921194	-1.792374	0.124760	0.039971	-0.045693
-0.090000	0.041315	0.068818	0.085297	-0.007606	-1.918517	-1.797930	0.141693	0.045688	-0.051839
-0.100000	0.041191	0.068728	0.084815	-0.008976	-1.915453	-1.804190	0.159129	0.051682	-0.058141
-0.110000	0.041054	0.068629	0.084289	-0.010538	-1.911974	-1.811171	0.177145	0.057998	-0.064616
-0.120000	0.040905	0.068522	0.083723	-0.012326	-1.908047	-1.818891	0.195822	0.064684	-0.071282
-0.130000	0.040744	0.068406	0.083118	-0.014380	-1.903634	-1.827373	0.215253	0.071797	-0.078157
-0.140000	0.040571	0.068281	0.082478	-0.016745	-1.898691	-1.836639	0.235539	0.079400	-0.085260
-0.150000	0.040386	0.068149	0.081806	-0.019474	-1.893166	-1.846715	0.256795	0.087566	-0.092608
-0.160000	0.040190	0.068009	0.081105	-0.022632	-1.886997	-1.857628	0.279152	0.096378	-0.100218
-0.170000	0.039983	0.067861	0.080378	-0.026292	-1.880113	-1.869409	0.302759	0.105932	-0.108107
-0.180000	0.039766	0.067706	0.079628	-0.030543	-1.872431	-1.882089	0.327788	0.116342	-0.116291
-0.190000	0.039538	0.067543	0.078861	-0.035493	-1.863850	-1.895703	0.354439	0.127738	-0.124786
-0.200000	0.039299	0.067374	0.078078	-0.041267	-1.854253	-1.910287	0.382949	0.140277	-0.133605

4.4.4 Continuation of Lyapunov orbits

Before seeing the behaviour of the manifolds of the Lyapunov orbits submitted to the effect of the parameter ε we are going to see how are these orbits in different levels of energy. In figure 4.34, different views of some falimies of Lyapunov orbits are shown. In all the cases, the Jacobi constant varies from $C = -0.20955$ to $C = -0.20855$.

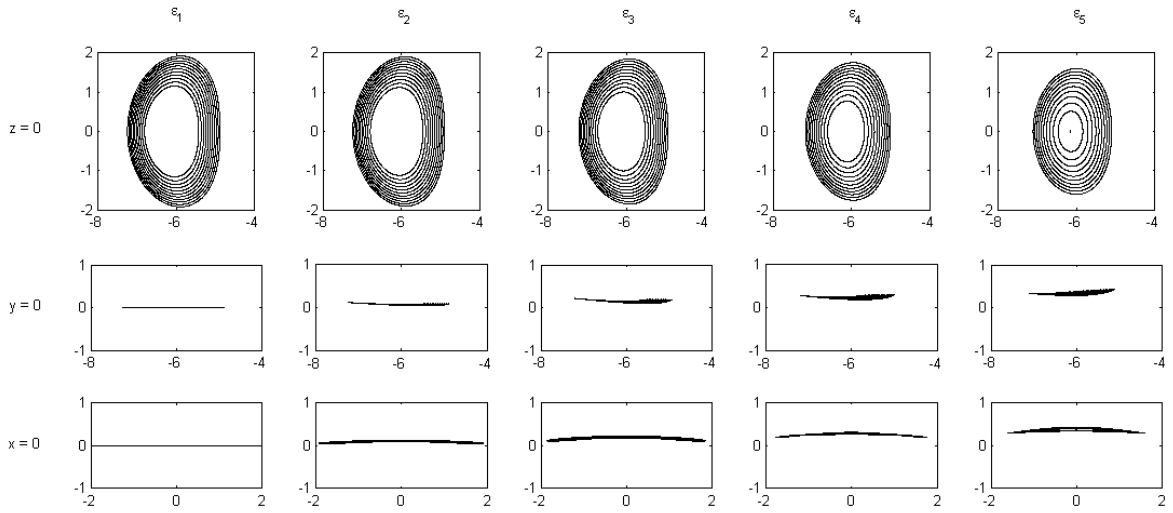

Figure 4.34. Different families of Lyapunov orbits. For a certain value of ε, each family has been obtained varying the Jacobi constant. $\varepsilon_1 = 0$, $\varepsilon_2 = -0.05$, $\varepsilon_3 = -0.1$, $\varepsilon_4 = -0.15$ and $\varepsilon_5 = -0.2$.

It can clearly be seen from the projection in the plane $y = 0$ that the orbits acquire some curvature while the parameter ε is increasing in norm. Moreover, the z component of these orbits rise because the bar has more inclination.

4.4.5 Stable and unstable manifolds

In this final section, we are going to present the results concerning the computations of the unstable manifold of Lyapunov periodic orbits around L_2 and L_3 ($\varepsilon = -0.2$). The stable case would be analogous. Figures 4.36 and 4.37 show the inner branches of these manifolds surrounding the bar in the inner region delimited by the zero-velocity surface. However, the interesting part is the outer branches. As in model 3 they spiral out like the spiral arms of a galaxy. It is thought that all the manifolds corresponding to the orbits around the critical points with different energies (figure 4.35) could form a path followed by lots of stars forming the spiral arms or the rings that we can observe in barred galaxies.

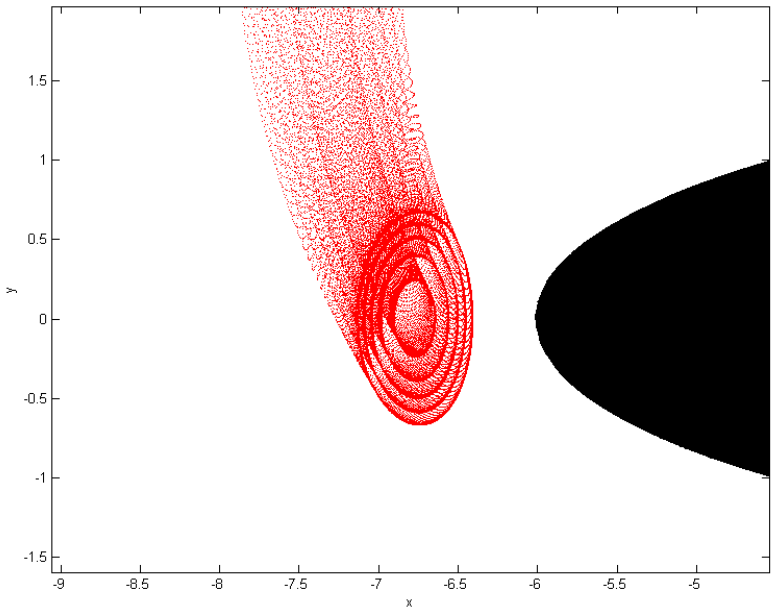

Figure 4.35. Unstable manifolds of different Lyapunov orbits near L_2.

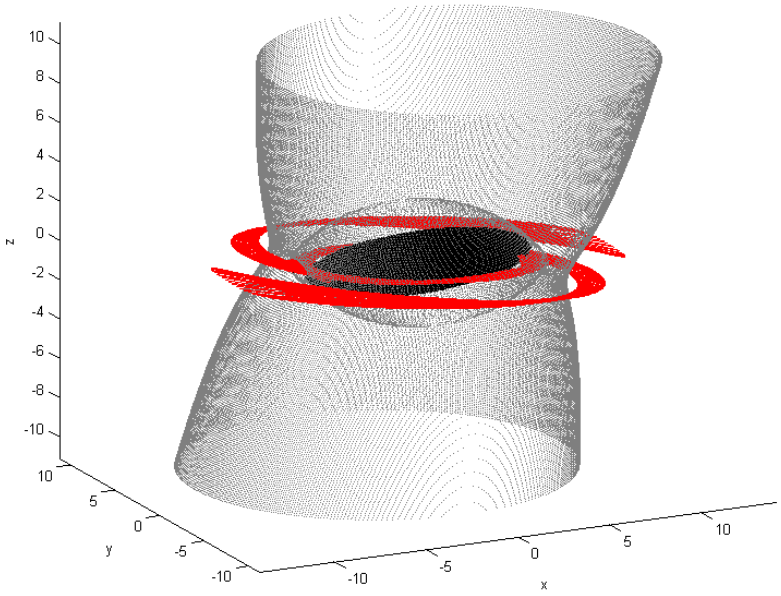

Figure 4.36. Unstable manifolds from Lyapunov orbits and the zero-velocity surface.

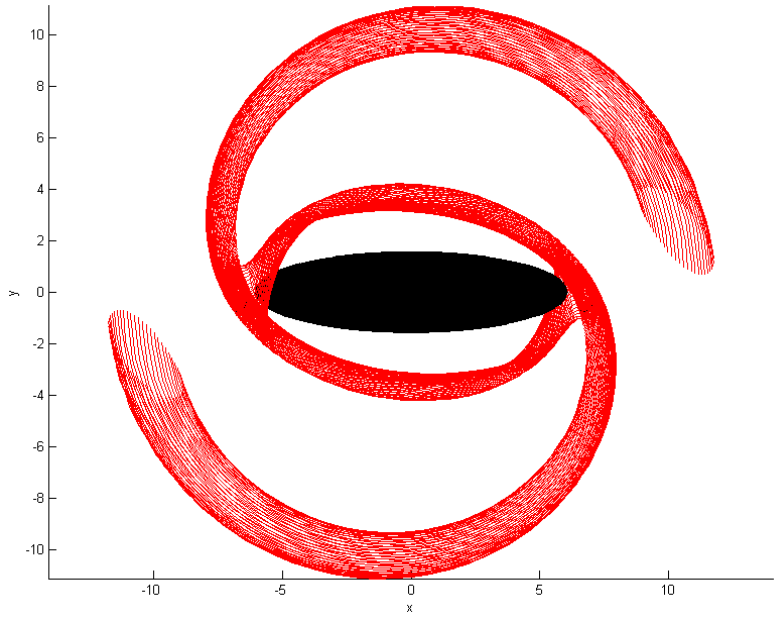

Figure 4.37. $x - y$ view of the unstable manifolds.

Seen in an edge-on position, these manifolds reveal the feature we were looking for. Indeed, the outer branches of the unstable manifold seem to be warped emulating the shape of some observed galaxies.

Comparing figure 4.38 with figure 4.39, it is obvious that there are similarities in the shape. Therefore, considering the precession like in this model could be a good approximation in order to model the galaxy warps. Further work can be focused in comparing and contrasting the results of the precessing model with real observations.

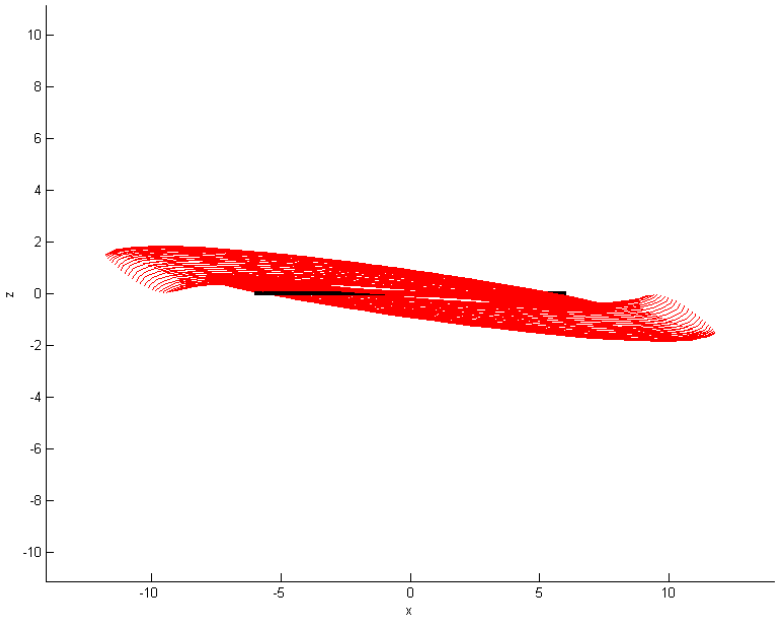

Figure 4.38. Edge-on view of the unstable manifolds.

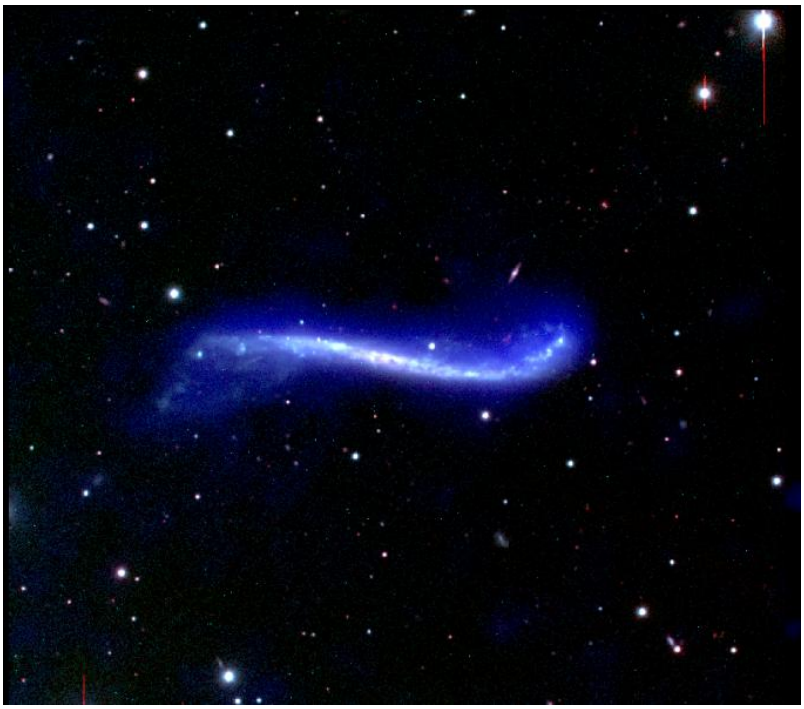

Figure 4.39. Galaxy UGC 3697.

5. Conclusions

The present project has resulted an introductory work about the precession phenomenon thought as a perturbation of basic models which have been widely studied.

The first approach to the problem led us to a model, the GP-RTBP, in which we were able to develop the equations of motion as it was made with the RTBP. We only had to take into account how the new synodic frame of reference moved with respect to the fixed one. It was there where the precession was introduced. In terms of numerical analysis we built some ad hoc procedures in order to compute the eight-shape periodic orbits which are the dynamical substitutes of the critical points due to the precession. The parallel shooting method was a powerful procedure to deal with the unstability of these orbits. The influence of the parameters of this model in the shape of the computed orbits was observed in some ranges of those parameters. Then, we noticed that for some values the method did not converge. With the purpose of determining the regions where the method diverged we decided to made a continuation map. It was necessary to take some grids in the domain with different distances among its points because of the problem of finding the best initial condition in the computation of an orbit. As a result, it was possible to see the tongue-like regions where the method found the periodic orbits.

After the first results we realized that the only way to explain this motion was by means of a force (or a torque). Because it was difficult to find a relationship between this force and a physical phenomenon, we focused in torque-free motions. Our intention was to study the most general torque-free motion of a rigid body. In the future model, the rigid body was thought as two spheres connected by a massless bar with the purpose of emulating the RTBP. However, torque-free motion implied that the movement of the primaries was in a circle like in the RTBP. At first, we introduced a torque causing a motion more similar to what we had in mind: both primaries oscillating. We obtained the equations of motion following the same procedure as it was done in the first model. The results obtained from this model, the RBAT-RTBP, led us to eight-shape periodic orbits too. Then, we computed the continuation map. Like the first model, this had the inconvenient of the applied torque. The second option in rigid body dynamics was to consider a torque-free motion of the primaries. In this way, the only possibility was to inflict to the bar which connected the spheres an inclination slightly lower than $\frac{\pi}{2}$. The resultant model, the RBTF-RTBP, autonomous after a short discussion, produced promising results. In first place the critical points were similar to those of the RTBP though the coordinates of some of them changed with respect to the parameter ε. Then, the zero-velocity curves obtained from the Jacobi constant had the particularity of being non-symmetric with respect the y axis for $z \neq 0$. In order to compute some invariant manifolds we obtained the horizontal Lyapunov orbits adapted to this perturbed RTBP

from their linear approximation. The procedure of refinement the linear Lyapunov orbits was a modified parallel shooting method introducing an equation for the energy. Once we had the orbits, the invariant stable and unstable manifolds came from computing the monodromy matrix of the orbits and transporting the eigenvectors related to the stable and unstable eigenvalues. In both models, it is important to remark that, despite the fact that we have been terming a precession phenomenon, the parameters were related to the nutation angle of the body.

In the last part of the work, we introduced the "precession" in a Miyamoto-Nagai Ferrers galactic model as in the RBTF-RTBP. Since the only difference was the potential it was easy to adapt the numerical procedures. We computed the critical points and the zero-velocity surfaces which preserved the disposition and shape observed in the RBTF-RTBP. Then, the Lyapunov orbits around the critical points were refined from the linear approximation. For significant values of ε we observed that these orbits cannot be embedded in any plane. Finally, we computed the stable and unstable manifolds for some cases and noticed that, seen in an edge-on position, these manifolds seem to be warped.

The different shapes of the galaxies has always been a matter of study. Concretely barred galaxies have some interesting features like the spiral arms, the rings, the ansae... Indeed, there are a lot of papers (some of them have been mentioned in the present work) which study the possible causes of these forms. The last part of this work has tried to find a possible explanation of the warp observed in some galaxies. This phenomenon could be more frequent than it seems since even our galaxy may be suffering a warp. For this reason, this matter could become an important subject of research. Here, we have used the stable and unstable manifold of some periodic orbits near the ends of the bar. These manifolds are influenced by the movement proposed to the bar, considered as a rigid body with torque-free motion, and they take that particular shape as the parameter increase in norm. Further work oriented in this matter could be based in contrasting the validity of the galactic model developed in this work with real observations.

6. References

[1] Athanassoula, E., Romero-Gómez, M., Masdemont, J.J., *Rings and spirals in barred galaxies - I. Building blocks*, Monthly Notices of the Royal Astronomical Society, 394, 67-81, 2009.

[2] Athanassoula, E., Romero-Gómez, M., Bosma, A., Masdemont, J.J., *Rings and spirals in barred galaxies - II. Ring and spiral morphology*, Monthly Notices of the Royal Astronomical Society, 400, 1706-1720, 2009.

[3] Athanassoula, E., Romero-Gómez, M., Bosma, A., Masdemont, J.J., *Rings and spirals in barred galaxies - III. Further comparisons and links to observations*, Monthly Notices of the Royal Astronomical Society, 407, 1433-1448, 2010.

[4] Bate, R., Mueller, D., White, J., *Fundamentals of astrodynamics*, Dover, New York, 1971.

[5] Buta, R., *The plume phenomenon in barred spirals*, Proceedings of the Astronomical Society of Australia, 5, 472-478, 1984.

[6] Buta, R., *The structure and dynamics of ringed galaxies. I - The morphology of galaxy rings, and statistics of their apparent shapes, relative sizes, and apparent orientations with respect to bars*, Astrophysical Journal Supplement, 61, 609-630, 1986.

[7] Buta, R. *The structure and dynamics of ringed galaxies. II. UBVRI surface photometry and H alpha kinematics of the ringed barred spiral NGC 1433*, Astrophysical Journal Supplement, 61, 631-665, 1986.

[8] Buta, R., *The catalog of southern ringed galaxies*, Astrophysical Journal Supplement, 96, 39-116, 1995.

[9] Buta, R. et al., *An optical, near-infrared, and kinematic study of four early-type resonance ring galaxies*, The Astronomical Journal, 116, 1142-1162, 1998.

[10] Ferrers, N.M., *An elementary treatise on spherical harmonics and subjects connected with them*, The Quarterly Journal of Pure and Applied Mathematics, 14, 1, 1877.

[11] Goldstein, H., Poole, C., Safko, J., *Classical mechanics*, 3rd ed., Addison-Wesley, San Francisco, 2002.

[12] Hand, L., Finch, J., *Analytical mechanics*, Cambridge University Press, Cambridge, 1998.

[13] López-Corredoira, M., Betancort-Rijo, J., Beckman, J.E., *Galactic disc warps due to intergalactic accretion flows onto the disc*, Astronomy and Astrophysics, 386, 169-186, 2002.

[14] Masdemont, J.J., *High-order expansions of invariant manifolds of libration point orbits with applications to mission design*, Dynamical Systems An International Journal, 20, 59-113, 2005.

[15] Romero-Gómez, M., *The role of invariant manifolds in the formation of spiral arms and rings in barred galaxies*, 2006.

[16] Romero-Gómez, M., Masdemont, J.J., Athanassoula, E., García-Gómez, C., *The origin of rR1 ring structures in barred galaxies*, Astronomy and Astrophysics, 453, 39-45, 2006.

[17] Romero-Gómez, M., Athanassoula, E., Masdemont, J.J., García-Gómez, C., *The formation of spiral arms and rings in barred galaxies*, Astronomy and Astrophysics, 472, 63-75, 2007.

[18] Schwarz, M.P., *The response of gas in a galactic disk to bar forcing*, The Astrophysical Journal, 247, 77-88, 1981.

[19] Schwarz, M.P., *How bar strength and pattern speed affect galactic spiral structure*, Monthly Notices of the Royal Astronomical Society, 209, 93-109, 1984.

[20] Schwarz, M.P., *A re-examination of some bar-driven models of spiral structure*, Monthly Notices of the Royal Astronomical Society, 212, 677-686, 1985.

[21] Szebehely, V., *Theory of orbits: the restricted problem of three bodies*, Academic Press, New York, 1967.